



Design, synthesis, and biological evaluation of a novel dual peroxisome proliferator-activated receptor alpha/delta agonist for the treatment of diabetic kidney disease through anti-inflammatory mechanisms



Kai Liu¹, Xing Zhao¹, Xue Qi¹, Dong-Liang Hou, Hao-Bin Li, Yu-Hao Gu, Qing-Long Xu^{*}

Jiangsu Key Laboratory of Drug Discovery for Metabolic Diseases, State Key Laboratory of Natural Medicines, China Pharmaceutical University, 24 Tongjia Xiang, Nanjing, 210009, China

ARTICLE INFO

Article history:

Received 7 February 2021

Received in revised form

8 March 2021

Accepted 14 March 2021

Available online 20 March 2021

Keywords:

PPAR

GFT505

Sulfuretin

Diabetic kidney disease

Inflammation

ABSTRACT

Diabetic kidney disease (DKD) is a major feature of the final stage of nearly all cause types of diabetes mellitus (DM). To date, few safe and effective drugs are available to treat. Peroxisome proliferator-activated receptors (PPARs), comprised of three members: PPAR- α , PPAR- δ and PPAR- γ , play a protective role in the DKD through glycemic control and lipid metabolism, whereas systemic activation of PPAR- γ causes serious side-effects in clinical trials. **GFT505** is a dual PPAR- α/δ agonist, and the selectivity against PPAR- γ is still to be improved. Sulfuretin has been shown to suppress the expression of PPAR- γ and improve the pathogenesis of diabetic complications. In this study, by hybridizing the carboxylic acid of **GFT505** and the parent nucleus of sulfuretin, we pioneeringly designed and synthesized a series of novel dual PPAR- α/δ agonists, expecting to provide a better benefit/risk ratio for PPARs. Of all the synthesized compounds, compound **12** was identified with highly activity on PPAR- α/δ and higher selectivity against PPAR- γ than that of **GFT505** (EC₅₀: hPPAR- α : 0.26 μ M vs.0.76 μ M; hPPAR- δ : 0.50 μ M vs.0.73 μ M; hPPAR- γ : 4.22 μ M vs.2.79 μ M). The molecular docking studies also depicted good binding affinity of compound **12** for PPAR- α and PPAR- δ compared to **GFT505**. Furthermore, compound **12** exhibited an evidently renoprotective effect on the DKD through inhibiting inflammatory process, which might at least partly *via* JNK/NF- κ B pathways *in vivo* and *in vitro*. Overall, compound **12** hold therapeutic promise for DKD.

© 2021 Elsevier Masson SAS. All rights reserved.

1. Introduction

Diabetic kidney disease (DKD), a serious complication of diabetes mellitus (DM), is one of the most leading causes of end-stage renal disease worldwide [1]. According to the 9th edition of Global Diabetes Map from the International Diabetes Federation (IDF) in 2019, approximately 463 million adults (20–79 years) were living with diabetes, by 2045 this will rise to 700 million. Seriously, up to 40% of people with diabetes will develop into DKD. Clinically, although several available therapeutic interventions, such as angiotensin converting enzyme inhibitors (ACEI) [2] or angiotensin II type 1 (AT1) receptor blockers [3], can delay the onset

progression of DKD, the morbidity and mortality associated with DKD remains high [4]. Research identifying additional therapeutic approaches that are innocuous is urgent clinical needs.

The pathogenesis of DKD is extremely complex involving multiply different pathways, including the glycolipid metabolism disorder [5], advanced glycation end products (AGEs) [6], protein kinase C [7], polyol pathway [8] and hemodynamic changes [9]. In parallel, compelling evidence supports the fact that inflammation plays a pivotal role in the development and progression of DKD [10]. The inflammatory infiltration, accumulation of macrophages, and increased secretion of injurious cytokines, including transforming growth factor β 1 (TGF- β 1), which is also a key regulator of extracellular matrix (ECM) protein synthesis in the progress of renal fibrosis, are observed in renal biopsy specimens from patients with DKD [11]. Therefore, inhibition of inflammation and the resulting ECM accumulation, may be served as a potential

* Corresponding author.

E-mail address: qlxu@cpu.edu.cn (Q.-L. Xu).

¹ These authors contributed equally to this article.

therapeutic approach for preventing kidney injury in DKD.

Peroxisome proliferator-activated receptors (PPARs) are ligand-activated transcription factors of nuclear hormone receptor superfamily, which comprises of three members: PPAR- α , PPAR- δ and PPAR- γ [12]. There is an increasing body of evidence suggesting that PPARs play a senior role in the pathogenesis of DKD for the function in glycemic control and lipid metabolism [13]. PPAR- α agonists are used as lipid lowering agents in clinical therapy for more than 30 years [14] and the anti-inflammatory effect of PPAR- δ agonists has been shown in many animal studies [15]. In addition, PPAR- γ agonists are widely used to control serum glucose levels of diabetic patients [16], nevertheless, several of them were discontinued because of PPAR- γ related weight gain, hemodilution and fluid retention in clinical trials [17]. It is mandatory to develop novel therapeutic interventions and simultaneous activation of PPAR- α/δ with higher selectivity against PPAR- γ may be a potential therapeutic option to prevent diabetes-associated hyperglycemia and hyperlipidemia provoked induction and progression of DKD.

GFT505 (Elafibranor, Fig. 1A), a PPARs agonist which exhibited preferential activity on PPAR- α/δ with no obvious PPAR- γ associated adverse effect, had been evaluated for the amelioration of glycolipid disorder associated with the metabolic syndrome several years [18] and exhibited reasonable effects on treatment of non-alcoholic steatohepatitis (NASH, NCT02704403, phase III) in clinical trials and DM in animal models [19]. But risks regarding adverse effects still exist for its activity on PPAR- γ . Developing dual PPAR α/δ agonists with minimum activity on PPAR- γ might be provide a better benefit/risk ratio in clinical practice. Moreover, it might be an innovative point of penetration to find a hybridizable molecule, which can antagonize PPAR- γ or inhibit the PPAR- γ expression in metabolic diseases. **Sulfuretin (Fig. 1B)**, one of the natural products isolated from *Rhus verniciflua*, exerted several pharmacological effects [20], including anti-inflammatory, anti-oxidation and anti-fibrosis, to improve the pathogenesis of diabetic complications in many animal studies [21,22]. More importantly, it is now increasingly appreciated that sulfuretin had potent anti-adipogenic activity *via* suppressing the expression of PPAR- γ in metabolic diseases [23,24], which indicated that sulfuretin might exist underlying connection with PPARs. Hence, we innovatively tried to hybridize the carboxylic acid of **GFT505** and the parent

nucleus of sulfuretin to design and synthesize a series of novel dual PPAR- α/δ agonists, expecting to increase the activity of PPAR- α/δ and simultaneously decrease the activation of PPAR- γ , as well as explore the pharmacological activity for diabetes-provoked induction and progression of DKD.

Taken together, in this study, we designed, synthesized a series of novel dual PPAR- α/δ agonists through hybridizing **GFT505** and sulfuretin, and evaluated their biological activities against PPARs, then screened promising candidates to verify potential binding mode for PPAR- α and PPAR- δ by molecular docking, as well as investigate the therapeutic efficacy and safety on the development of DKD *in vivo* and *in vitro*.

2. Results and discussion

2.1. Chemistry

The target compounds **1–16** were prepared *via* a convergent synthesis according to the synthetic route outlined in **Schemes 1**. The compound **B** were synthesized through 3,5-dimethyl-4-hydroxybenzaldehyde (**A**) and ethyl 2-bromoisobutyrate in acetonitrile containing caesium carbonate. Then the aldehyde **B** was reduced to give alcohol **C** in the presence of sodium borohydride. Subsequently, in the presence of carbon tetrabromide and triphenylphosphine, the compound **D** was obtained in 50% yield over 3 steps. On the other hand, the compound **F** were synthesized by condensation of the corresponding aldehyde with 6-hydroxy-2,3-dihydrobenzo[b]furan-3-one (**E**) under basic condition. Then the compound **F** reacted with **D** in acetonitrile afforded the corresponding acetate **G**. Finally, the acetate **G** was then carried out in the presence of potassium hydroxide to afford the desired compounds **1–16** (**Scheme 1**).

2.2. PPARs agonistic activity

Compounds **1–16** were evaluated *in vitro* for their agonistic activities toward the human PPAR- α , PPAR- δ and PPAR- γ subtypes by employing GAL4-PPAR transactivation assay in transiently transfected COS7 cells. Commercially available PPAR agonists, GW7647 (**Fig. 1C**), GW501516 (**Fig. 1D**) and rosiglitazone (**Fig. 1E**),

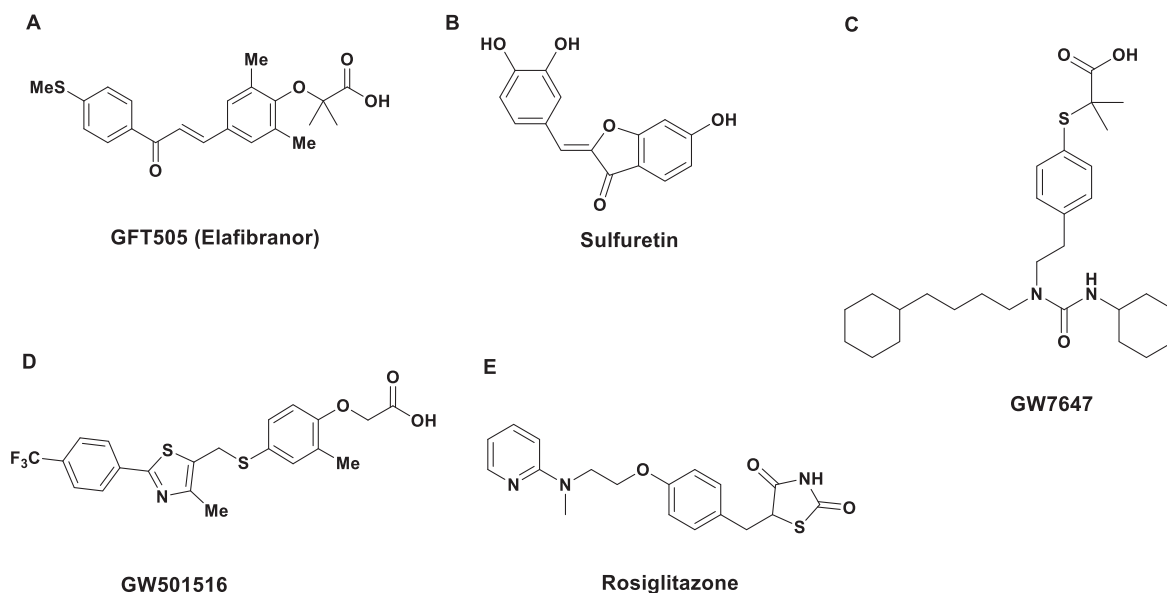
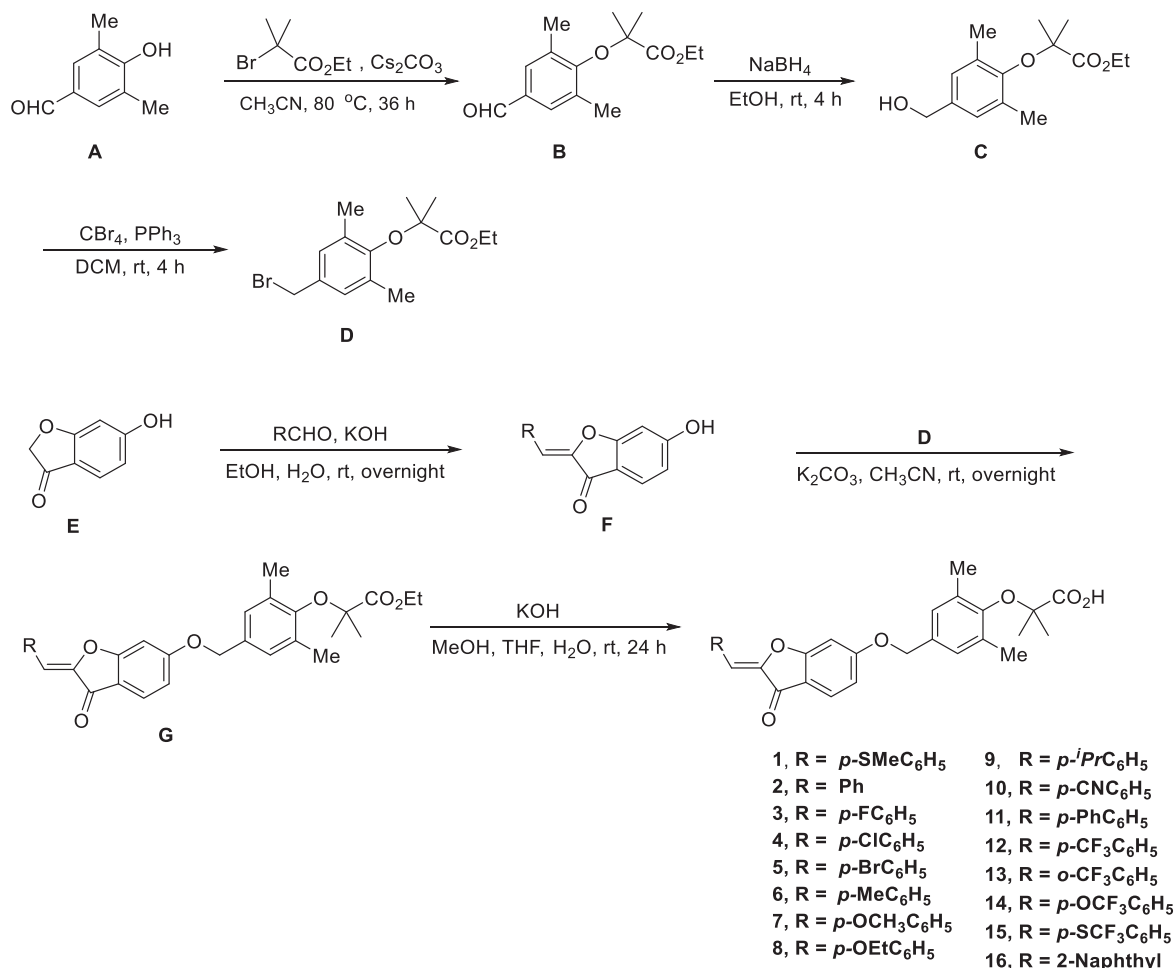


Fig. 1. Structure of **GFT505** (Elafibranor), sulfuretin, GW7647, GW501516 and rosiglitazone.



Scheme 1. Synthetic route for target product 1–16.

were used as reference compounds for PPAR- α , PPAR- δ and PPAR- γ

Table 1
In vitro activities of the human PPARs. ^a

Compd.	hPPAR- α (EC ₅₀)	hPPAR- δ (EC ₅₀)	hPPAR- γ (EC ₅₀)
GFT505	0.76 ± 0.15 μ M	0.73 ± 0.17 μ M	2.79 ± 0.35 μ M
1	3.10 ± 0.96 μ M	1.80 ± 0.34 μ M	1.72 ± 0.24 μ M
2	2.80 ± 0.47 μ M	1.60 ± 0.42 μ M	>10 μ M
3	>10 μ M	>10 μ M	>10 μ M
4	1.73 ± 0.48 μ M	1.98 ± 0.16 μ M	>10 μ M
5	0.79 ± 0.01 μ M	1.72 ± 0.45 μ M	>10 μ M
6	5.21 ± 0.12 μ M	3.93 ± 0.62 μ M	>10 μ M
7	>10 μ M	2.25 ± 0.61 μ M	>10 μ M
8	>10 μ M	2.31 ± 0.18 μ M	>10 μ M
9	3.30 ± 0.14 μ M	0.52 ± 0.02 μ M	>10 μ M
10	4.44 ± 0.90 μ M	8.94 ± 2.65 μ M	>10 μ M
11	1.88 ± 0.49 μ M	2.45 ± 0.03 μ M	1.00 ± 0.02 μ M
12	0.26 ± 0.08 μ M	0.50 ± 0.10 μ M	4.22 ± 0.18 μ M
13	1.66 ± 0.12 μ M	1.63 ± 0.29 μ M	>10 μ M
14	1.03 ± 0.18 μ M	1.17 ± 0.16 μ M	6.36 ± 1.50 μ M
15	4.56 ± 1.70 μ M	1.26 ± 0.25 μ M	1.63 ± 0.40 μ M
16	4.19 ± 1.87 μ M	0.98 ± 0.24 μ M	>10 μ M
GW7647	2.08 ± 0.48 nM	ND	ND
GW501516	ND ^b	1.05 ± 0.37 nM	ND
Rosiglitazone	ND	ND	191.50 ± 46.67 nM

^a EC₅₀ value represent the mean of at least two determinations, which is the concentration giving 50% of the maximal activity determined for the tested compound.

^b ND: not determined.

activity, respectively. The results were summarized in Table 1. Among all the synthesized compounds, compound **12** exhibited the best agonistic activity towards PPAR- α and PPAR- δ . It exerted PPAR- α and PPAR- δ agonistic activation 16.2-fold and 8.4-fold greater than PPAR- γ activity, respectively. More importantly, compound **12** exhibited more potent than PPAR- α/δ agonistic activity with higher selectivity against PPAR- γ compared to **GFT505** (EC₅₀: hPPAR- α : 0.26 μ M vs.0.76 μ M; hPPAR- δ : 0.50 μ M vs.0.73 μ M; hPPAR- γ : 4.22 μ M vs.2.79 μ M), respectively. Above all, compound **12** was optimal, providing potent PPAR- α/δ activity and high PPAR- α/δ selectivity against PPAR- γ .

2.3. Molecular docking study

To get a more detailed view at a molecular level of compound **12** acting on PPAR- α and PPAR- δ , molecular docking study was performed, **GFT-505** was also studied in the same protocol for comparison. As shown in Fig. 2, **GFT-505** and compound **12** were docked into the binding sites of PPAR- α (Fig. 2 and 2B) and PPAR- δ (Fig. 2C and 2D), respectively. The predicted binding modes between compound **12** and PPAR- α showed that hydrogen bond interactions were generated between the ligand and Ser 280, Tyr314, His 440 and Tyr464 (Fig. 2B). The predicted binding mode between compound **12** and PPAR- δ showed that hydrogen bond interactions were generated between the ligand and Thr252, Thr253, His 287, His 413 and Tyr437 (Fig. 2D). Compound **12** kept all the protein-

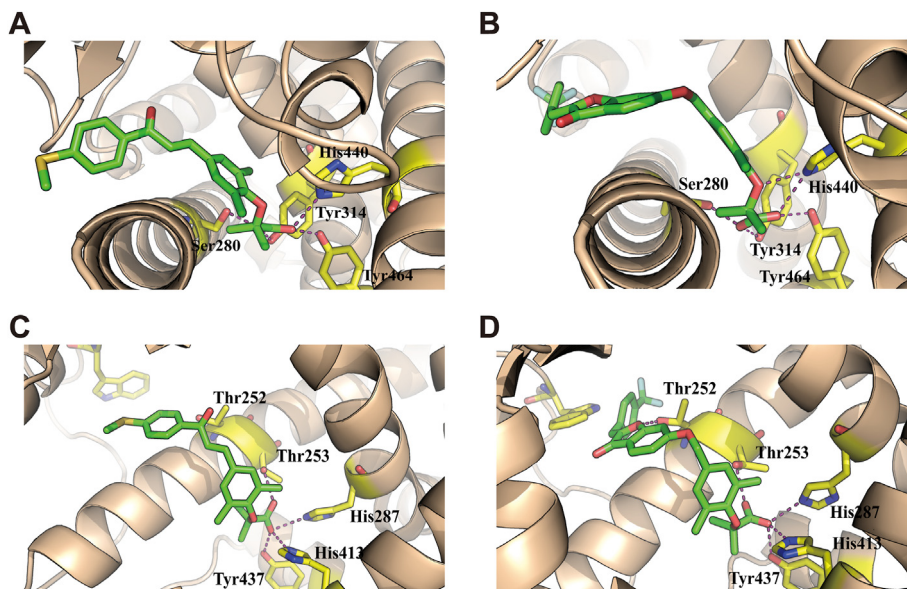


Fig. 2. The binding model of **GFT-505** (A,C) and compound **12** (B,D) in the pocket of PPAR- α (A ~ B) and PPAR- δ (C ~ D) was predicted by molecular docking. The PPAR- α or PPAR- δ protein was shown in wheat carton. Green stick: small molecules, Yellow stick: key amino acid residues, Magenta dash: hydrogen bonds.

ligand interactions of **GFT-505** with all the key residues of PPAR- α and PPAR- δ , indicating its potential bioactivity against these two subtypes of PPAR. Hence, we selected compound **12** as the promising candidate to investigate therapeutic efficacy and safety on the development of DKD *in vivo* and *in vitro*.

2.4. Pharmacodynamic evaluation *in vivo* and *in vitro*

2.4.1. Effects on the general symptoms in DKD rats

Initially, we examined the effects of compound **12** on the fasting blood glucose and body weight in model rats during the animal procedures. Results showed that the model rats had the symptoms of hyperglycemia and weight loss which are typical characteristics of DM. There was no significant difference in fasting blood glucose between the four DKD groups (Fig. 3A). In parallel, the decrease of body weight in model rats tended to be less with compound **12** treatment, but this trend was not statistically significant (Fig. 3B). However, results of renal morphology showed that the kidneys from model rats were obvious swelling and exhibited brownish yellow compared with the control which were vivid purple brown. Treatment with compound **12** at two doses obviously ameliorated this symptom (Fig. 3C). Moreover, compound **12** treatment significantly reduced the kidney/body weight ratio compared to the model group (Fig. 3D). Collectively, these data revealed that DM occurred in rats and suggested that compound **12** might ameliorate nephrosis in DKD rats without depending on hypoglycemic action.

2.4.2. Effects on renal functional parameters in DKD rats

Next, we evaluated the effects of compound **12** on renal functional parameters in DKD rats. We determined the 24 h albuminuria during the experiments and found that it was significantly increased in model rats as compared with that in control rats. Interestingly, administration of compound **12** for 6 weeks significantly attenuated the DM induced increment in 24 h albuminuria (Fig. 3E). At the end of experiments, we also determined the serum levels of urea nitrogen, creatinine and cystatin C, three key parameters of renal function. Compound **12** at two doses significantly reduced the serum levels of urea nitrogen and creatinine, to different degrees compared to the model rats (Fig. 3F and 3G).

Furthermore, the evidently elevated serum cystatin C observed in the model rats was apparently attenuated in the compound **12** treated rats (Fig. 3H). Taken together, these data revealed that DKD occurred in rats and suggested that compound **12** could protect renal functions in DKD rats.

2.4.3. Effects on lipid metabolism in DKD rats

Excess intracellular lipid accumulation in non-adipose tissue, such as in kidney, can induce cell injury and organ dysfunction (termed lipotoxicity) [25]. We found that the serum levels of triglyceride (TG) and total cholesterol (TC) were significantly higher in model rats than in control rats (Fig. 4A and 4B). However, compound **12** at two doses significantly reduced the serum TG levels (Fig. 4A). The increase of TC was tended to be less with compound **12** treatment, but this trend was not statistically significant (Fig. 4B). Furthermore, the renal Oil red O staining results showed that compound **12** treatment evidently decreased the excess intracellular lipid accumulation in the renal of model rats (Fig. 4C). Consistently, this finding was supported by the decreased contents of TG and TC in serum. To verify the effect of compound **12** treatment on hepatotoxicity, the serum levels of alanine aminotransferase (ALT) and aspartate aminotransferase (AST) were measured. The results showed that compound **12** treatment did not increase the serum levels of ALT and AST, but slightly decreased the level of AST (Fig. 4D and 4E), indicating no obvious hepatotoxicity of compound **12** at these two doses. Altogether, these data revealed that compound **12** at these two doses could restore lipid metabolic disorder in DKD rats to different degrees.

2.4.4. Effects on oxidative stress in DKD rats

Lipid peroxidation (LPO) is always potentiated by oxidative stress [26] and accumulating evidence also indicate that activation of oxidative stress plays a key role in kidney further aggravating DKD [27]. Considering compound **12** could restore lipid metabolic disorder, we thus measured serum and kidney levels of malondialdehyde (MDA) and superoxide dismutase (SOD), two major parameters for oxidative stress. We found a marked increase in serum and kidney levels of MDA in model rats, which was blunted by compound **12** treatment (Fig. 4F). In parallel, the serum and

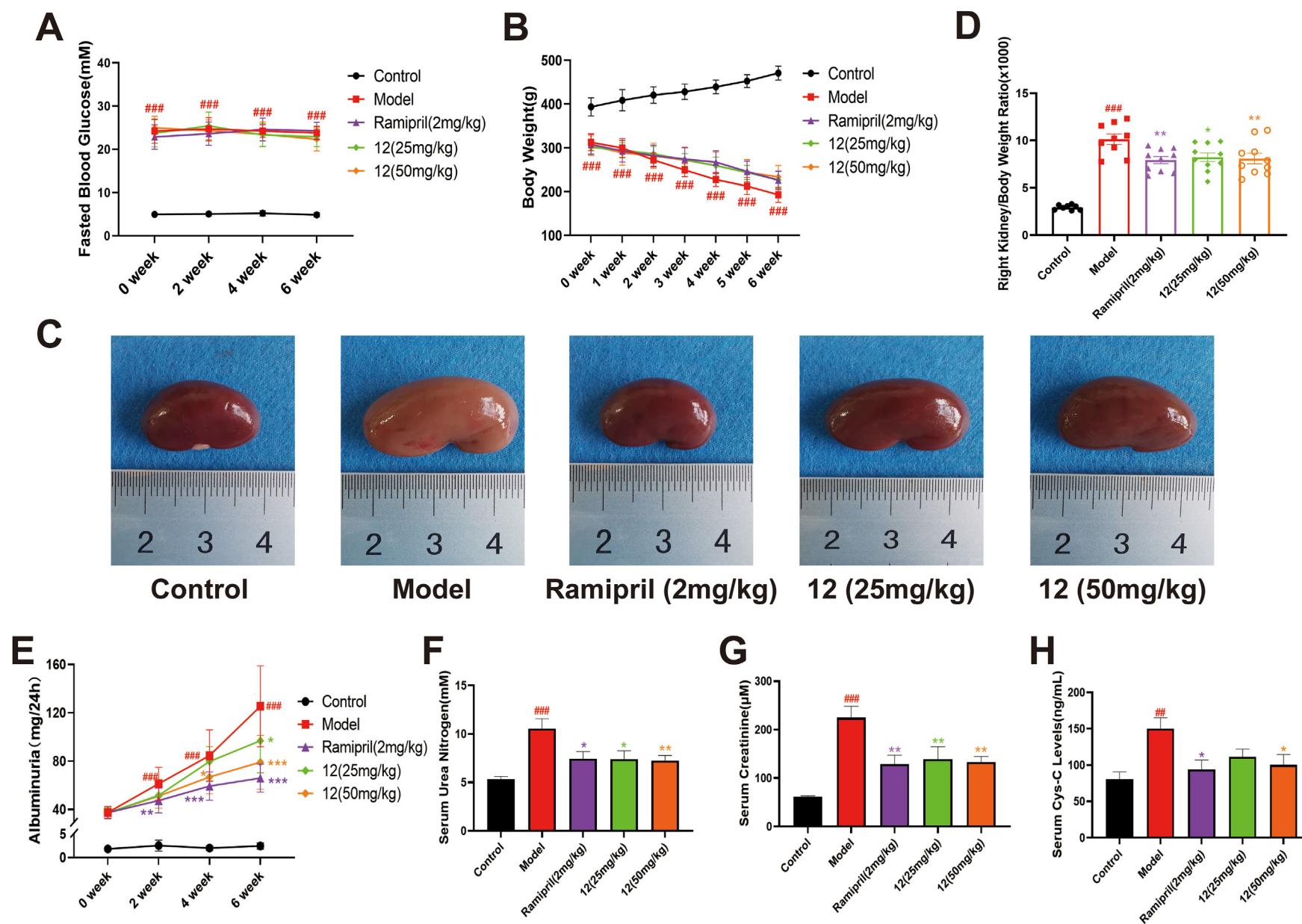


Fig. 3. Effects on the general symptoms and renal functional parameters in DKD rats. (A) Measurement of fasting blood glucose levels at weeks 0, 2, 4 and 6 during the experiments. (B) Measurement of body weight at weeks 0, 1, 2, 3, 4, 5 and 6 during the experiments. (C) Representative renal morphology of rats at the end of the experiments. (D) Measurement of right kidney/body weight ratio at the end of the experiments. (E) Measurement of 24 h albuminuria at weeks 0, 2, 4 and 6 during the experiments. (F) Measurement of serum urea nitrogen at the end of the experiments. (G) Measurement of serum creatinine at the end of the experiments. (H) Measurement of serum cystatin C at the end of the experiments. All data were presented as means \pm SEM ($n = 8-10$ per group). Statistical significance of differences were determined by one-way ANOVA. ### $p < 0.001$ and ## $p < 0.01$ compared to Control group; *** $p < 0.001$, ** $p < 0.01$ and * $p < 0.05$ compared to Model group.

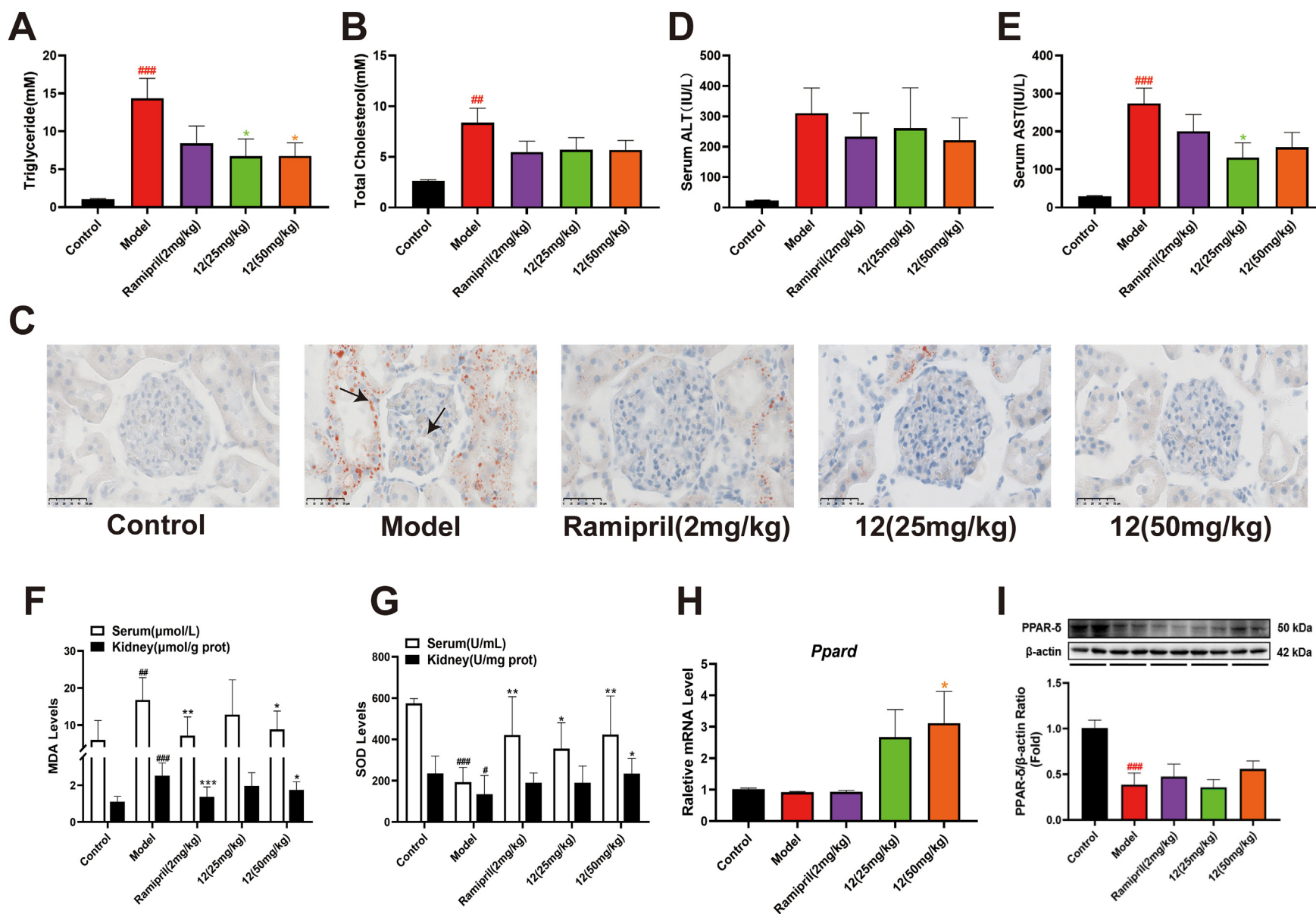


Fig. 4. Effects on lipid metabolism, oxidative stress and PPAR- δ expression in DKD rats. (A) Measurement of serum TG at the end of the experiments. (B) Measurement of serum TC at the end of the experiments. (C) Representative sections of Oil red O staining on the renal cortex of DKD rats. Scale bars, 50 μ m. (D) Measurement of serum ALT at the end of the experiments. (E) Measurement of serum AST at the end of the experiments. (F) Measurement of the levels of serum and kidney MDA at the end of the experiments. (G) Measurement of the levels of serum and kidney SOD at the end of the experiments. (H) RT-PCR analyses of *Ppard* mRNA expression in renal cortex of DKD rats. β -actin was used as the invariant control. (I) Western blot analyses of PPAR- δ protein expression in renal cortex of DKD rats. β -actin was used as an invariant control for equal loading. Representative blots are shown with densitometry. All data were presented as means \pm SEM (n = 8–10 per group). Statistical significance of differences were determined by one-way ANOVA. ###p < 0.001 and ##p < 0.01 compared to Control group; ***p < 0.001, **p < 0.01 and *p < 0.05 compared to Model group.

kidney activity of SOD was noted to be decreased in model rats compared to control rats. However, compound **12** at the high dose significantly restored the decreased SOD activity in both serum and kidney (Fig. 4G), suggesting that oxidative stress could be attenuated by compound **12** treatment. Taken together, these data indicated that compound **12** may improve LPO via suppressing the oxidative stress in serum and kidney, which may contribute to the improved renal function in DKD rats.

2.4.5. Effects on the PPAR- δ expression in the kidney of DKD rats

It is worth-mentioning that PPARs are expressed in several tissues including the kidney. PPAR- α is predominantly expressed in proximal tubules and medullary thick ascending limbs, PPAR- γ is selectively expressed in medullary collecting ducts, glomeruli and pelvic urothelium, while PPAR- δ is equally expressed in renal cortex and medulla [28]. Notably, numerous clinical cases and literatures [29,30] had revealed that glomerulosclerosis in the renal cortex is the source of the genesis and progression of DKD and the renal cortex was widely investigated for molecular mechanisms of DKD. We therefore detected the PPAR- α and PPAR- δ expression in the renal cortex. Consistently, the mRNA level of PPAR- α was undetectable in the renal cortex. There was no changes in renal cortex PPAR- δ mRNA expression between the control and model rats. However, the PPAR- δ mRNA of compound **12** at two doses had significantly high expression compared to another groups, even had significant difference at high dose compared to the model group (Fig. 4H). Furthermore, determination of PPAR- δ protein expression in the renal cortex showed that the protein levels were all significantly depressed in the DKD rats. The decrease of PPAR- δ protein expression in DKD rats tended to be less with compound **12** treatment, but this trend was not statistically significant (Fig. 4I). Currently, the literatures about PPAR- δ agonists on the expression of PPAR- δ are few and controversial. Data from studies by Liang et al. [28] and Lee et al. [31] were almost consistent with us. On the contrary, Matsushita et al. [15] found that the renal PPAR- δ mRNA and protein expression were significantly greater in the DM group than in the control group. The reason for the divergence was unknown. A possible explanation for this might be that the stability of PPAR- δ protein in DKD might be altered [32,33].

2.4.6. Effects on the inflammatory response in the kidney of DKD rats

Many studies have proposed an important role of inflammatory processes in the pathogenesis of DKD [34]. Tumor necrosis factor α (TNF- α), interleukin-1 β (IL-1 β) and interleukin 6 (IL-6), as important inflammatory factors, are involved in the inflammatory pathological damage process in DKD patients [35]. We thereby detected mRNA expression of the three factors to evaluate the occurrence of inflammation *in vivo*. As shown in Fig. 5, the mRNA expression TNF- α in the model rats were expressively up-regulated in contrast with the control rats. But compound **12** at two doses were significantly down-regulated the mRNA expression TNF- α (Fig. 5A). The increase of mRNA expression of IL-1 β and IL-6 in model rats was not statistically significant, but this trend tended to be less with compound **12** treatment (Fig. 5B and 5C). Meanwhile, we detected the effects of compound **12** on macrophage infiltration in the kidney. CD14 is a marker for all macrophages, and CD11c is specific for the M1 subtype of macrophages [15]. We found that the mRNA levels of CD11c and CD14, were strongly increased in the model group. However, compound **12** treatment significantly reduced the expression of CD11c and slightly decreased the expression of CD14 (Fig. 5D and 5E). Further histological evidence strengthened the protective role of compound **12** for the kidney through anti-inflammatory mechanism. Data from hematoxylin and eosin (HE) staining revealed that obvious inflammatory infiltration and

lesions, cells disordered arrangement, spotty necrosis and vacuolar degeneration occurred in kidney from model rats. Nonetheless, these pathological alterations were markedly improved by compound **12** at two doses (Fig. 5F). Collectively, these data clearly indicated that compound **12** could suppress the inflammatory process in the kidney of DKD rats.

2.4.7. Effects on the fibrosis response in the kidney of DKD rats

Renal fibrosis is also a primary characteristic of advanced DKD and the process is usually irreversible [36]. Notably, ECM accumulation is the major cause of renal fibrosis [37]. We initially used periodic acid-Schiff (PAS) staining to determine the structure of glomerulus and Masson's trichrome staining to assess the accumulation of ECM. As shown in Fig. 6, obvious accumulation of glycogen, mesangial expansion and collagen deposition were found in the kidney of model rats. Intriguingly, the DKD-induced these pathological lesions were significantly improved by compound **12** at two doses to different degrees (Fig. 6A-6C). To further validate the improvements of compound **12** on renal fibrosis in DKD rats, we detected the mRNA expression of TGF- β 1, collagen4a1, laminin, connective tissue growth factor (CTGF), osteopontin (OPN), and plasminogen activator inhibitor-1(PAI-1), which were fibrosis-related factors during renal fibrosis [38]. Consistent with the changes of the mesangial fractional and interstitial fibrosis area, gene expression for this six parameters were markedly increased in model rats, and dramatically suppressed by compound **12** at two doses treatment to different degrees (Fig. 6D-6I). Noteworthy, excessive TGF- β 1 is associated with ECM collagen 4 in the glomerular area and both have been identified as key mediators of glomerular and tubulointerstitial pathologies in DKD [39]. Immunohistochemical analyses showed that the protein expression of TGF- β 1 and collagen 4 was evidently increased in the model rats as compared to the control rats. However, both were expressed at significantly lower levels in the compound **12** groups (Fig. 6J-6L). Above all, these results suggested that compound **12** might lead to decrease renal fibrosis in DKD rats through inhibiting relevant fibrosis-related factors pathological overexpression.

2.4.8. Effects on the inflammatory and fibrosis response *in vitro*

To further validate the anti-inflammatory and anti-fibrosis effects of compound **12** on DKD, we examined *in vitro* anti-inflammatory and anti-fibrosis activity of compound **12** in human glomerular mesangial cells (HGMCs), which are known to regulate the secretion of ECM in kidney [28], and human myeloid leukemia mononuclear cells (THP-1)-derived macrophages. We firstly evaluated the effects of compound **12** at different concentrations (1, 3, 10, 30 μ M) on cell viability. Results showed that exposure of HGMCs and THP-1-derived macrophages to 1, 3, 10 or 30 μ M of compound **12** did not affect cell viability at 48 h (Fig. 7A-7B). Then, we examined the effects of compound **12** on the anti-inflammatory and anti-fibrosis activity in corresponding cells. As expected, compound **12** significantly inhibited high glucose (HG)-induced mRNA expression of TGF- β 1 (Fig. 7C). Moreover, Lipopolysaccharide (LPS)-induced mRNA expression of TGF- β 1, TNF- α , even IL-1 β and IL-6, in THP-1-derived macrophages were markedly down-regulated by compound **12** in a dose-dependent manner (Fig. 7D-7G). However, it seemed that compound **12** could not suppress the mRNA expression of collagen1a1, collagen4a1, laminin and CTGF, which can be induced by TGF- β 1 in HGMCs (Fig. 7H-7K). Collectively, these data indicated that compound **12** strongly inhibited HG and LPS induced inflammatory gene expression, which might be a potential way to ameliorate renal functions in DKD, rather than directly suppressing fibrosis-related factors.

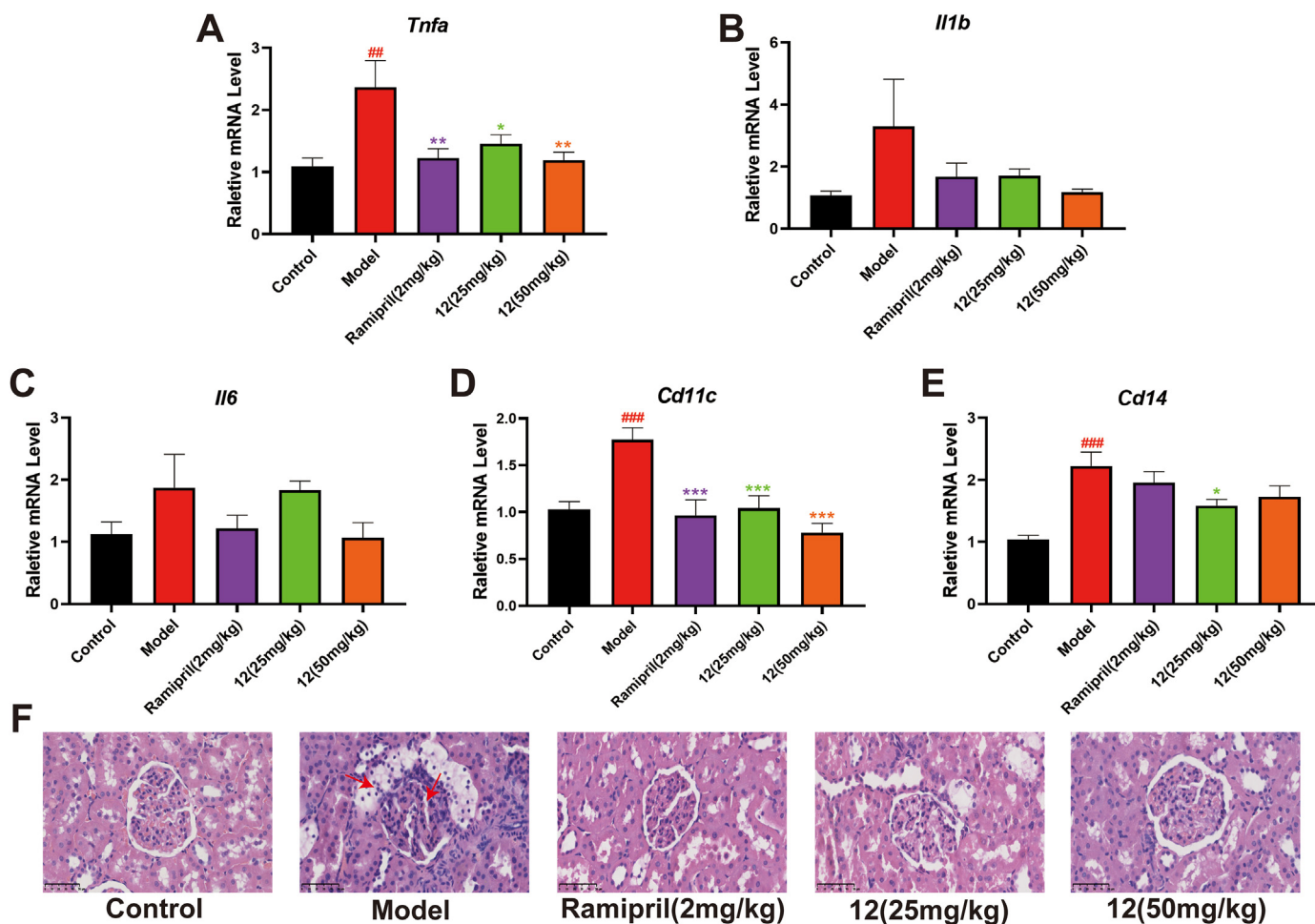


Fig. 5. Effects on the inflammatory response in the kidney of DKD rats. RT-PCR analyses of *Tnfa* (A), *Il1b* (B), *Il-6* (C), *Cd11c* (D), *Cd14* (E) mRNA expression in renal cortex of DKD rats. β -actin was used as the invariant control. (F) Representative sections of HE staining on the renal cortex of DKD rats. Scale bars, 50 μ m. All data were presented as means \pm SEM (n = 8–10 per group). Statistical significance of differences were determined by one-way ANOVA. ###p < 0.001 and ##p < 0.01 compared to Control group; ***p < 0.001, **p < 0.01 and *p < 0.05 compared to Model group.

2.4.9. Preliminary study on anti-inflammatory mechanism

Finally, we preliminarily tried to explore the anti-inflammatory mechanism of compound **12** on DKD. Among the known factors that are incriminated in the genesis and progression of DKD, the c-Jun N-terminal protein kinase (JNK) and nuclear transcription factor kappa B (NF- κ B) play crucial roles in the pathogenesis of DKD via inflammatory process [40,41]. Of note, both PPARs [42] and sulfuretin [20] had been shown to suppress inflammation process through down-regulation of these two factors in many DM animal studies. We thus checked the phosphorylation levels of JNK and NF- κ B in HG-induced HGMCs and THP-1-derived macrophages stimulated by LPS. Immunoblot analysis demonstrated that the DMSO group had significantly high phosphorylation levels of JNK and NF- κ B in both HGMCs and macrophages compared to the control group. The increase of phosphorylation levels of JNK and NF- κ B were tended to be less with compound **12** groups, but this trend was not statistically significant in HGMCs (Fig. 8A–8C). However, intriguingly, when we investigated the dose-dependent effects of compound **12** on LPS-induced macrophages, a simultaneous and significant decrease of phosphorylation levels of JNK and NF- κ B were observed (Fig. 8D–8F). Subsequently, to further validate the potential anti-inflammatory mechanism *in vitro*, we detected the phosphorylation levels of JNK and NF- κ B in the kidney of DKD rats. As expected, immunoblot analysis showed that phosphorylation

levels of the two factors were all significantly elevated in the model rats, but were clearly dose dependently decreased by treatment with compound **12** compared to the model rats (Fig. 8G–8I). Together, these data indicated that compound **12** could suppress JNK and NF- κ B signaling pathways *in vivo* and *in vitro*, which may be, at least partly, a potential molecular mechanism to ameliorate inflammatory process for DKD.

2.5. Discussion

As potential targets for the therapy of DKD, PPARs are critically involved in the regulation of metabolic syndrome which associated with glucose and lipid metabolism. Numerous preclinical studies detected PPAR- α agonists, such as fenofibrate (Fig. 9A) and bezafibrate (Fig. 9B), had positive renal effects on the animals with DKD. The activation of PPAR- α regulated responsible for LPO and oxidative stress [43]. Moreover, the expression of TGF- β could also be attenuated via PPAR- α activation, which led to improved renal fibrosis [44]. Meanwhile, thirteen trials of the 290 clinical studies revealed fenofibrate consistently reduced the progression of urinary albumin excretion in the DM patients [45]. However, further research on this series of agonists was prevented because of associating with serum creatinine level increasing in clinical trials [46], indicating current therapeutic limitations of the use of PPAR- α .

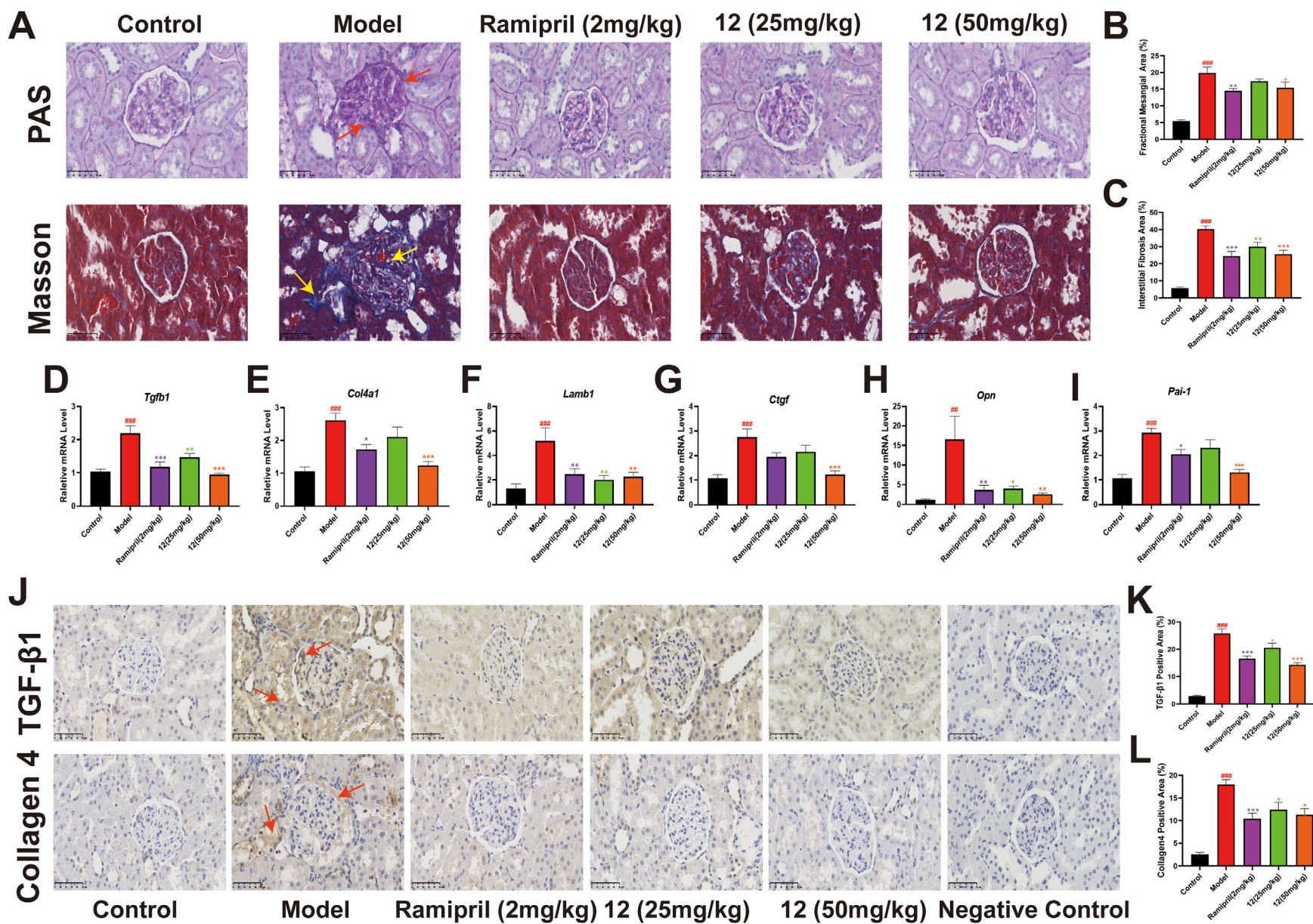


Fig. 6. Effects on the fibrosis response in the kidney of DKD rats. (A) Representative sections of PAS and Masson's trichrome staining on the renal cortex of DKD rats. Scale bars, 50 μ m. (B) Quantitative analysis of the positive mesangial fractional area (%). (C) Quantitative analysis of the positive interstitial fibrosis area (%). RT-PCR analyses of *Tgfb1*(D), *Col4a1* (E), *Lamb 1* (F), *Ctgf* (G), *Opn* (H) and *Pai-1*(I) mRNA expression in renal cortex of DKD rats. β -actin was used as the invariant control. (J) Representative immunohistochemistry sections for TGF- β 1 and collagen4 on the renal cortex of DKD rats. Scale bars, 50 μ m. (K) Quantitative analysis of the positive (stained) area for TGF- β 1 area (%). (L) Quantitative analysis of the positive (stained) area for collagen4 area (%). All data were presented as means \pm SEM (n = 8–10 per group). Statistical significance of differences were determined by one-way ANOVA. ###p < 0.001, ##p < 0.01 compared to Control group; ***p < 0.001, **p < 0.01 and *p < 0.05 compared to Model group.

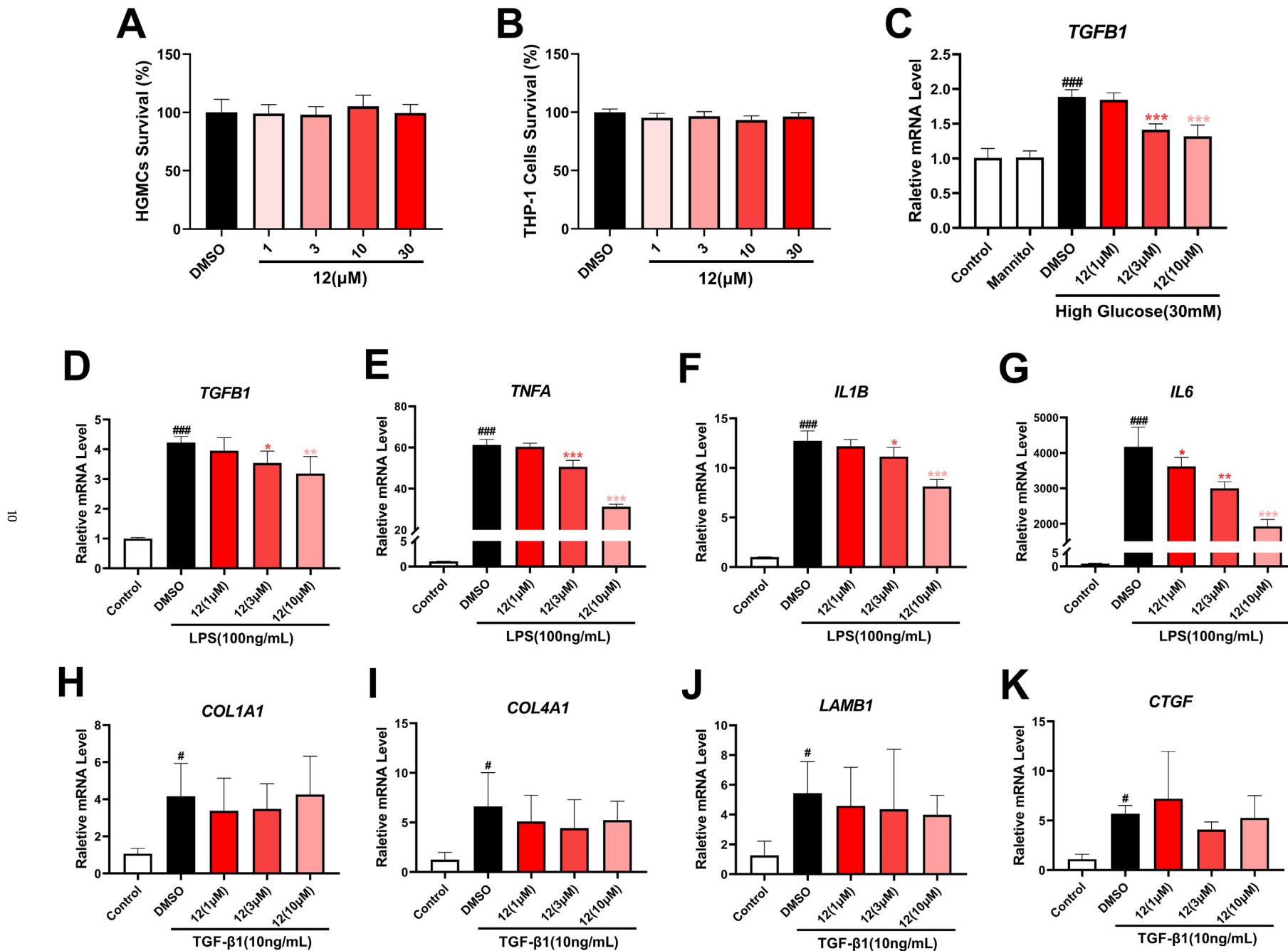


Fig. 7. Effects on cell viability, inflammatory and fibrosis response in HGMCs and THP-1-derived macrophages. (A) Effects on cell viability in HGMCs. (B) Effects on cell viability in THP-1-derived macrophages. (C) RT-PCR analyses of *TGFB1* mRNA expression in HGMCs. RT-PCR analyses of *TGFB1* (D), *TNFA* (E), *IL1B* (F) and *IL6* (G) mRNA expression in THP-1-derived macrophages. RT-PCR analyses of *COL1A1* (H), *COL4A1* (I), *LAMB1* (J) and *CTGF* (K) mRNA expression in HGMC. β -actin was used as the invariant control. All data were presented as means \pm SEM (n = 5 per group). Statistical significance of differences were determined by one-way ANOVA. ###p < 0.001 and #p < 0.05 compared to Control group; ***p < 0.001, **p < 0.01 and *p < 0.05 compared to DMSO group.

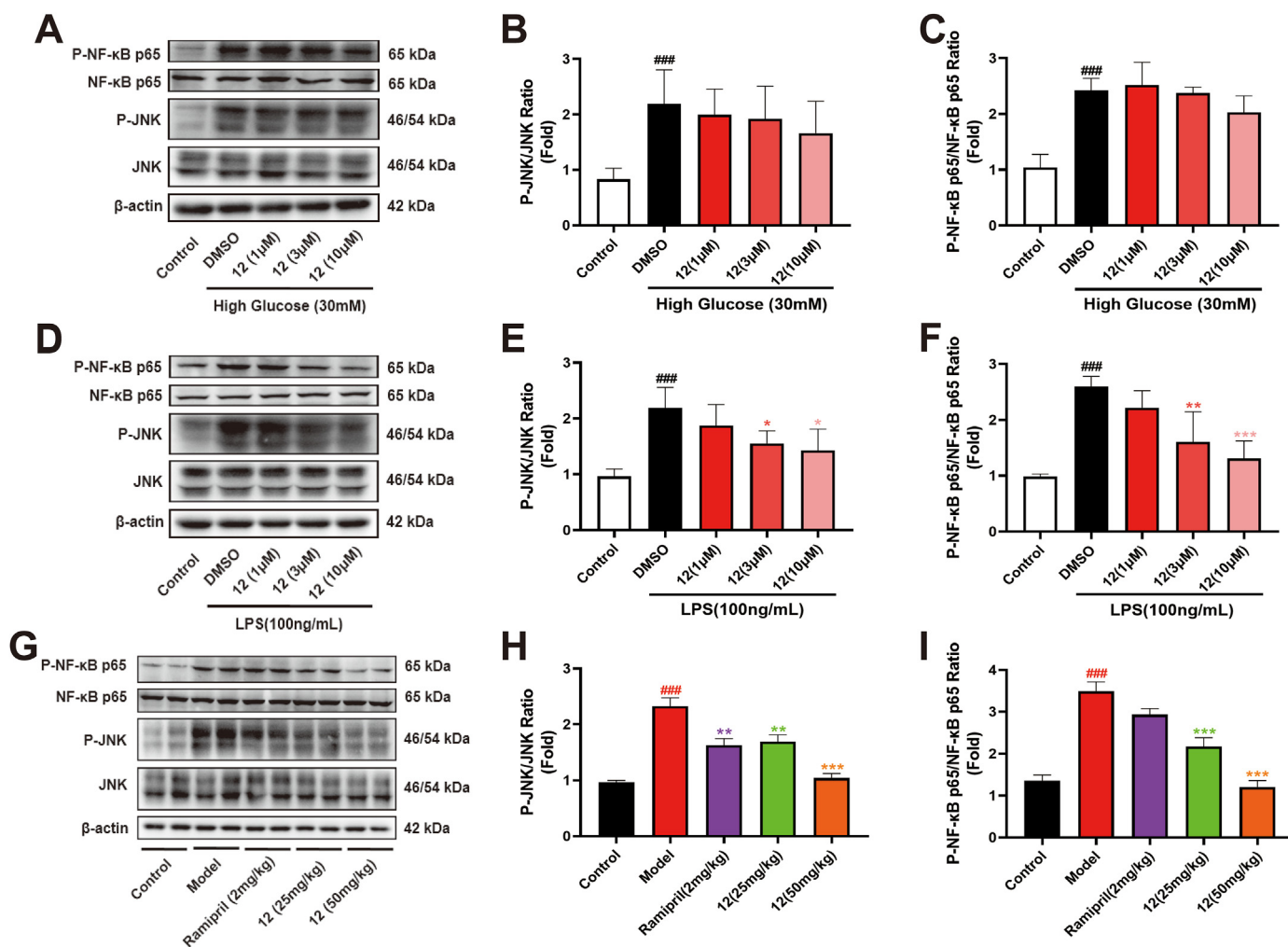


Fig. 8. Preliminary study on anti-inflammatory mechanism. (A) Representative western blots for P-NF-κB p65, NF-κB p65, P-JNK, JNK protein expression in HG-induced HGMCs. (B) Quantitative analyses for P-JNK/JNK in HG-induced HGMCs. (C) Quantitative analyses for P-NF-κB p65/NF-κB p65 in HG-induced HGMCs. (D) Representative western blots for P-NF-κB p65, NF-κB p65, P-JNK, JNK protein expression in THP-1-derived macrophages stimulated by LPS. (E) Quantitative analyses for P-JNK/JNK in THP-1-derived macrophages stimulated by LPS. (F) Quantitative analyses for P-NF-κB p65/NF-κB p65 in THP-1-derived macrophages stimulated by LPS. (G) Representative western blots for P-NF-κB p65, NF-κB p65, P-JNK, JNK protein expression in the renal cortex of DKD rats. (H) Quantitative analyses for P-JNK/JNK in the renal cortex of DKD rats. (I) Quantitative analyses for P-NF-κB p65/NF-κB p65 in the renal cortex of DKD rats. β-actin was used as an invariant control for equal loading. All data were presented as means ± SEM (n = 3 per group in cells and n = 8–10 per group in rats). Statistical significance of differences were determined by one-way ANOVA. ^{###}p < 0.001 compared to Control group; ^{***}p < 0.001, ^{**}p < 0.01 and ^{*}p < 0.05 compared to DMSO or Model group.

agonists. Compared with PPAR-α agonists, compound **12** at doses of 25 mg/kg and 50 mg/kg also effectively improved the DKD characteristic symptoms. Notably, decreased the serum level of creatinine (Fig. 3G) was observed, which successfully circumvented the side-effect from PPAR-α agonists (fibrates).

Currently, studies on the effects of PPAR-δ agonists for the DKD are still rare. Matsushita et al. [15] and Lee et al. [31] found GW0742 (Fig. 9C), a PPAR-δ agonist, could suppress the gene expression of inflammatory mediators and prevent nephrin loss in the renal cortex without altering blood glucose levels. Liang et al. [28] reported L-165041 (Fig. 9D), another PPAR-δ agonist, could improve DKD *in vivo* associated with inhibition of AGEs and NF-κB pathways. Intriguingly, similar effects also had been demonstrated from compound **12**. It markedly suppressed the gene expression of inflammatory cytokines and attenuated the inflammatory response in kidney of DKD rats, might at least partly *via* JNK/NF-κB pathways *in vivo* and *in vitro*, indicating the role played by PPAR-δ agonists was ideally manifested.

For years, synthetic PPAR-γ (rosiglitazone) [47], dual PPAR-α/γ

(aleglitazar, Fig. 9E) [48], dual PPAR-δ/γ ([5-(Benzyloxy)-1H-indol-1-yl] acetic acid, Fig. 9F) [49] and pan-PPARα/δ/γ (chigliptazar, Fig. 9G) [50] agonists had also been developed to treat DM or DKD. However, most of them were prevented because of PPAR-γ related weight gain, fluid reaction, hemodilution and edema effect [17,51].

Considering the current research status surrounding the PPARs agonists' intervention for DKD, compound **12**, which was pioneeringly designed and synthesized *via* hybridizing the carboxylic acid of **GFT505** and the parent nucleus of sulfuretin, showed distinct advantages in not only PPARs agonistic activities but also therapeutic efficacy for DKD. More importantly, it successfully preserved the advantages of PPAR-α and PPAR-δ agonists while circumventing the side-effect from PPAR-α agonists, holding therapeutic potential against DKD.

3. Conclusion

In summary, a novel dual PPAR-α/δ agonist was discovered through hybridizing the carboxylic acids of **GFT505** and the parent

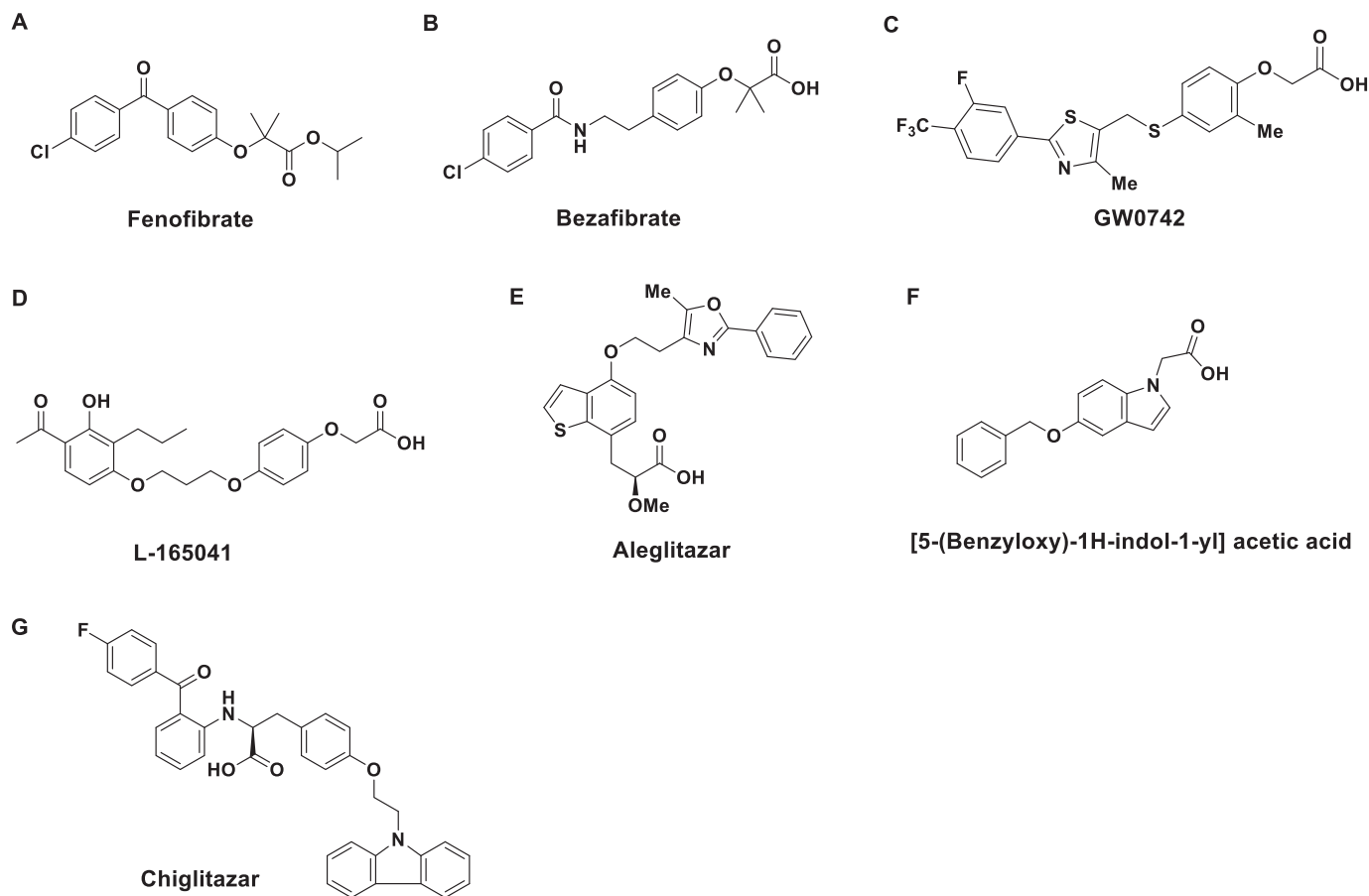


Fig. 9. Structure of PPARs agonists.

nucleus of sulfuretin. Compound **12** exhibited more potent than PPAR- α/δ agonistic activity with higher selectivity against PPAR- γ compared to **GFT505** (EC_{50} : hPPAR- α : 0.26 μ M vs. 0.76 μ M; hPPAR- δ : 0.50 μ M vs. 0.73 μ M; hPPAR- γ : 4.22 μ M vs. 2.79 μ M). In addition, molecular docking study showed that compound **12** kept all the protein-ligand interactions of **GFT-505** with all the key residues of PPAR- α and PPAR- δ , indicating its potential bioactivity against these two subtypes of PPAR. Furthermore, compound **12** was not only capable of attenuating the characteristic symptoms from DKD while circumventing the side-effect from PPAR- α agonists, but also orchestrating inflammation and fibrosis responses, which might at least partly via JNK/NF- κ B pathways *in vivo* and *in vitro*. Overall, compound **12** successfully took the essence and discarded the dregs from PPARs, holding therapeutic promise for DKD.

4. Experimental section

4.1. General chemistry

All reagents solvents used in this study were commercially purchased products with purity $\geq 95\%$. Analytical thin-layer chromatography (TLC) was performed on silica gel 60 F254 plates (Qingdao Ocean Chemical Company, China). Column chromatography was carried out on silica gel (200–300 mesh, Qingdao Ocean Chemical Company, China). ^1H and ^{13}C NMR spectra were performed on an ACF*300Q Bruker spectrometer with Me $_4$ Si as the internal reference. Proton coupling patterns were described as singlet (s), doublet (d), doublet of doublets (dd), triplet (t), triplet of

doublets (td), quartet (q), multiplet (m), and broad (br). Low and high resolution mass spectra (LRMS and HRMS) were given with electrospray ionization (ESI) produced by Waters Q-TOF Micro and Agilent G6230B, respectively. Melting points (mp) were measured in open capillary tubes, using an RY-1G melting point apparatus (0–300 $^{\circ}\text{C}$). All target compounds were confirmed with over 95% purity by UPLC. A Waters Acquity UPLC system comprising the Quaternary Solvent manager, Sample Manager-FTN, PDA Detector were employed. The UPLC conditions were as follows: ACQUITY UPLC $^{\text{®}}$ BEH C18 column, 2.1 \times 50 mm, 1.7 μm ; detection wavelength: 254 nm. Water and methanol containing 0.05% formic acid were used to perform elution at a flow rate of 1.2 mL/min.

4.1.1. General synthetic procedure for intermediates D

A round-bottomed flask was charged with 3,5-dimethyl-4-hydroxybenzaldehyde (**A**, 1.0 equiv.) and ethyl 2-bromoisobutyrate (3.0 equiv.), caesium carbonate (3.0 equiv.), solved in acetonitrile. The reaction mixture was stirred at 80 $^{\circ}\text{C}$ for 36 h. After the reaction was completed (monitored by TLC), the mixture was diluted by water and extracted by ethyl acetate. The combined organic layer was washed with brine, dried over anhydrous sodium sulfate and concentrated under the reduced pressure. The corresponding compound **B** was used in the next step without further purification.

In a dry round-bottomed flask, compound **B** (1.0 equiv.) in ethanol was cooled at 0 $^{\circ}\text{C}$. sodium borohydride (1.0 equiv.) was added in portions. The mixture was reacted for 4 h at room temperature. After the reaction was completed (monitored by TLC),

water was added slowly at 0 °C. The mixture was stirred for 15 min, then the mixture was extracted by ethyl acetate. The combined organic layer was washed with brine, dried over anhydrous sodium sulfate and concentrated under the reduced pressure. The corresponding compound **C** was used in the next step without further purification.

In a dry round-bottomed flask, compound **C** (1.0 equiv.) and carbon tetrabromide (1.5 equiv.) solved in dichloromethane was cooled at 0 °C. Triphenylphosphine (1.3 equiv.) solved in dichloromethane was added dropwise. The mixture was reacted for 4 h at room temperature. The reaction was removed solid by filtration, then the filtrate was evaporated under reduced pressure and purified by flash chromatography on silica gel (petroleum ether/ethyl acetate = 10:1) to afford the corresponding product **D**.

4.1.2. General synthetic procedure for targets 1-16

In a dry round-bottomed flask, 6-hydroxy-2,3-dihydrobenzo[b]furan-3-one (**E**, 1.0 equiv.) and substituted benzaldehyde (1.5 equiv.), potassium hydroxide (1.0 equiv.) solved in ethanol, then the mixture was reacted overnight at room temperature. After the reaction was completed (monitored by TLC), con. hydrochloric acid was added slowly at 0 °C. The solid was precipitated from the mixture, the corresponding product **F** was obtained by filtration.

In a dry round-bottomed flask, compound **F** (1.0 equiv.), compound **D** (1.5 equiv.) and potassium carbonate (2.0 equiv.) was solved in acetonitrile, then the mixture was reacted overnight. The mixture was evaporated under reduced pressure and purified by flash chromatography on silica gel (petroleum ether/ethyl acetate = 10:1) to afford the corresponding product **G**.

In a dry round-bottomed flask, compound **G** (1.0 equiv.), potassium hydroxide (3.0 equiv.) was solved in tetrahydrofuran/methanol/water, then the mixture was reacted at room temperature. After the reaction was completed (monitored by TLC), 1.0 M hydrochloric acid was added to adjust the mixture to PH = 5–6. Then the mixture was extracted by dichloromethane. The combined organic layer was washed with brine, dried over anhydrous sodium sulfate and concentrated under the reduced pressure, then purified by flash chromatography on silica gel (dichloromethane/methanol = 200:1) to afford the product (**1–16**).

4.1.2.1. (*Z*)-2-(2,6-dimethyl-4-(((2-(4-(methylthio)benzylidene)-3-oxo-2,3-dihydrobenzofuran-6-yl)oxy)methyl)phenoxy)-2-methylpropanoic acid (**1**). 32% Yield, yellow solid. ¹H NMR (500 MHz, DMSO-*d*₆) δ 7.90 (d, *J* = 8.3 Hz, 2H), 7.69 (d, *J* = 8.6 Hz, 1H), 7.37 (d, *J* = 8.3 Hz, 2H), 7.22 (s, 1H), 7.12 (s, 2H), 6.92 (d, *J* = 8.4 Hz, 1H), 6.83 (s, 1H), 5.13 (s, 2H), 2.54 (s, 3H), 2.20 (s, 6H), 1.36 (s, 6H). ¹³C NMR (126 MHz, DMSO-*d*₆) δ 181.41, 167.67, 166.39, 152.84, 146.84, 141.38, 132.67, 131.49, 130.70, 128.45, 128.20, 125.61, 125.43, 114.05, 113.12, 110.88, 97.78, 80.51, 70.23, 25.19, 17.64, 14.09. HRMS (ESI) exact mass calcd for C₂₉H₂₉O₆S requires *m/z* 505.1685, found 505.1681.

4.1.2.2. (*Z*)-2-(4-(((2-benzylidene-3-oxo-2,3-dihydrobenzofuran-6-yl)oxy)methyl)-2,6-dimethylphenoxy)-2-methylpropanoic acid (**2**). 36% Yield, white solid. ¹H NMR (500 MHz, DMSO-*d*₆) δ 12.91 (s, 1H), 7.98 (d, *J* = 7.4 Hz, 2H), 7.71 (d, *J* = 8.5 Hz, 1H), 7.55–7.45 (m, 3H), 7.25 (s, 1H), 7.14 (s, 2H), 6.93 (d, *J* = 8.4 Hz, 1H), 6.86 (s, 1H), 5.14 (s, 2H), 2.21 (s, 6H), 1.39 (s, 6H). ¹³C NMR (126 MHz, DMSO-*d*₆) δ 181.64, 175.08, 167.98, 166.52, 152.59, 147.26, 132.61, 131.98, 131.12, 130.89, 129.79, 128.96, 128.50, 125.52, 113.91, 113.18, 110.92, 97.83, 80.15, 70.20, 24.95, 17.57. HRMS (ESI) exact mass calcd for C₂₈H₂₇O₆ requires *m/z* 459.1808, found 459.1804.

4.1.2.3. (*Z*)-2-(4-(((2-(4-fluorobenzylidene)-3-oxo-2,3-dihydrobenzofuran-6-yl)oxy)methyl)-2,6-dimethylphenoxy)-2-

methylpropanoic acid (**3**). 38% Yield, white solid. ¹H NMR (500 MHz, DMSO-*d*₆) δ 12.90 (br s, 1H), 8.15–7.98 (m, 2H), 7.69 (d, *J* = 8.5 Hz, 1H), 7.35 (t, *J* = 8.5 Hz, 2H), 7.21 (s, 1H), 7.13 (s, 2H), 6.91 (d, *J* = 8.4 Hz, 1H), 6.87 (s, 1H), 5.12 (s, 2H), 2.20 (s, 6H), 1.38 (s, 6H). ¹³C NMR (126 MHz, DMSO-*d*₆) δ 181.57, 175.12, 167.21 (d, *J* = 179.9 Hz), 163.61, 161.63, 152.61, 146.93, 133.43 (d, *J* = 8.5 Hz), 132.62, 130.87, 128.66 (d, *J* = 2.5 Hz), 128.50, 125.52, 116.09 (d, *J* = 21.6 Hz), 113.92, 113.19, 109.85, 97.79, 80.17, 70.20, 24.97, 17.58. HRMS (ESI) exact mass calcd for C₂₈H₂₆FO₆ requires *m/z* 477.1713, found 477.1710.

4.1.2.4. (*Z*)-2-(4-(((2-(4-cholobenzylidene)-3-oxo-2,3-dihydrobenzofuran-6-yl)oxy)methyl)-2,6-dimethylphenoxy)-2-methylpropanoic acid (**4**). 38% Yield, white solid. ¹H NMR (500 MHz, DMSO-*d*₆) δ 12.84 (br s, 1H), 7.98 (d, *J* = 8.1 Hz, 1H), 7.71 (d, *J* = 8.5 Hz, 1H), 7.57 (d, *J* = 8.1 Hz, 1H), 7.23 (s, 1H), 7.13 (s, 2H), 6.93 (d, *J* = 8.1 Hz, 1H), 6.87 (s, 1H), 5.14 (s, 2H), 2.21 (s, 6H), 1.38 (s, 6H). ¹³C NMR (126 MHz, DMSO-*d*₆) δ 181.52, 167.95, 166.58, 152.63, 147.45, 134.35, 132.64, 132.62, 130.94, 130.83, 129.03, 128.47, 125.57, 113.81, 113.28, 109.53, 97.82, 80.20, 70.23, 24.99, 17.58. HRMS (ESI) exact mass calcd for C₂₈H₂₆ClO₆ requires *m/z* 493.1411, found 493.1418.

4.1.2.5. (*Z*)-2-(4-(((2-(4-bromobenzylidene)-3-oxo-2,3-dihydrobenzofuran-6-yl)oxy)methyl)-2,6-dimethylphenoxy)-2-methylpropanoic acid (**5**). 35% Yield, yellow solid. ¹H NMR (500 MHz, DMSO-*d*₆) δ 12.89 (br s, 1H), 7.88 (d, *J* = 8.2 Hz, 2H), 7.68 (d, *J* = 8.4 Hz, 2H), 7.19 (s, 1H), 7.12 (s, 1H), 6.90 (d, *J* = 8.3 Hz, 1H), 6.82 (s, 1H), 5.12 (s, 2H), 2.19 (s, 6H), 1.37 (s, 6H). ¹³C NMR (126 MHz, DMSO-*d*₆) δ 182.01, 175.60, 168.42, 167.06, 153.10, 148.00, 133.31, 133.11, 132.44, 131.74, 131.34, 128.97, 126.05, 123.75, 114.29, 113.77, 110.10, 98.28, 80.66, 70.71, 25.46, 18.07. HRMS (ESI) exact mass calcd for C₂₈H₂₆BrO₆ requires *m/z* 537.0913, found 537.0914.

4.1.2.6. (*Z*)-2-(2,6-dimethyl-4-(((2-(4-methylbenzylidene)-3-oxo-2,3-dihydrobenzofuran-6-yl)oxy)methyl)phenoxy)-2-methylpropanoic acid (**6**). 33% Yield, white solid. ¹H NMR (500 MHz, DMSO-*d*₆) δ 12.81 (br s, 1H), 7.88 (d, *J* = 8.0 Hz, 2H), 7.70 (d, *J* = 8.6 Hz, 1H), 7.33 (d, *J* = 7.9 Hz, 2H), 7.26 (s, 1H), 7.13 (s, 2H), 6.92 (d, *J* = 6.6 Hz, 1H), 6.83 (s, 1H), 5.14 (s, 2H), 2.37 (s, 3H), 2.20 (s, 6H), 1.38 (s, 6H). ¹³C NMR (126 MHz, DMSO-*d*₆) δ 181.57, 175.10, 167.83, 166.42, 152.59, 146.82, 139.94, 132.61, 131.17, 130.91, 129.64, 129.19, 128.49, 125.44, 114.02, 113.15, 111.18, 97.79, 80.16, 70.19, 24.97, 21.12, 17.58. HRMS (ESI) exact mass calcd for C₂₉H₂₉O₆ requires *m/z* 473.1964, found 473.1960.

4.1.2.7. (*Z*)-2-(4-(((2-(4-methoxybenzylidene)-3-oxo-2,3-dihydrobenzofuran-6-yl)oxy)methyl)-2,6-dimethylphenoxy)-2-methylpropanoic acid (**7**). 37% Yield, white solid. ¹H NMR (500 MHz, DMSO-*d*₆) δ 12.89 (br s, 1H), 7.96 (d, *J* = 8.7 Hz, 2H), 7.70 (d, *J* = 8.5 Hz, 1H), 7.23 (s, 1H), 7.14 (s, 1H), 7.09 (d, *J* = 8.7 Hz, 2H), 6.98–6.91 (m, 1H), 6.86 (s, 1H), 5.14 (s, 2H), 3.85 (s, 3H), 2.21 (s, 6H), 1.39 (s, 6H). ¹³C NMR (126 MHz, DMSO-*d*₆) δ 181.40, 175.07, 167.59, 166.23, 160.61, 152.56, 146.06, 133.06, 132.60, 130.95, 128.50, 125.35, 124.49, 114.62, 114.22, 113.01, 111.39, 97.76, 80.14, 70.15, 55.36, 24.95, 17.57. HRMS (ESI) exact mass calcd for C₂₉H₂₉O₇ requires *m/z* 489.1913, found 489.1911.

4.1.2.8. (*Z*)-2-(4-(((2-(4-ethoxybenzylidene)-3-oxo-2,3-dihydrobenzofuran-6-yl)oxy)methyl)-2,6-dimethylphenoxy)-2-methylpropanoic acid (**8**). 32% Yield, yellow solid. ¹H NMR (500 MHz, DMSO-*d*₆) δ 12.90 (br s, 1H), 7.95 (d, *J* = 8.6 Hz, 2H), 7.70 (d, *J* = 8.6 Hz, 1H), 7.24 (s, 1H), 7.14 (s, 2H), 7.07 (d, *J* = 8.6 Hz, 2H), 6.93 (d, *J* = 8.5 Hz, 1H), 6.85 (s, 1H), 5.14 (s, 2H), 4.12 (d, *J* = 7.0 Hz, 2H), 2.21 (s, 6H), 1.38 (s, 6H), 1.36 (t, *J* = 7.2 Hz, 3H). ¹³C NMR

(126 MHz, DMSO- d_6) δ 181.40, 175.10, 167.59, 166.24, 159.93, 152.60, 146.02, 133.10, 132.61, 130.93, 128.50, 125.35, 124.33, 115.01, 114.23, 113.03, 111.46, 97.75, 80.18, 70.16, 63.35, 24.98, 17.58, 14.50. HRMS (ESI) exact mass calcd for $C_{30}H_{31}O_7$ requires m/z 503.2070, found 503.2066.

4.1.2.9. (*Z*)-2-(4-(((2-(4-isopropylbenzylidene)-3-oxo-2,3-dihydrobenzofuran-6-yl)oxy)methyl)-2,6-dimethylphenoxy)-2-methylpropanoic acid (9). 40% Yield, yellow solid. 1H NMR (500 MHz, DMSO- d_6) δ 12.91 (br s, 1H), 7.91 (d, $J = 7.8$ Hz, 2H), 7.72 (d, $J = 8.4$ Hz, 1H), 7.40 (d, $J = 7.8$ Hz, 1H), 7.25 (s, 1H), 7.15 (s, 2H), 6.94 (d, $J = 8.4$ Hz, 1H), 6.85 (s, 1H), 5.16 (s, 2H), 3.03–2.90 (m, 1H), 2.21 (s, 6H), 1.39 (s, 6H), 1.25 (d, $J = 6.7$ Hz, 6H). ^{13}C NMR (126 MHz, DMSO- d_6) δ 181.58, 175.09, 167.85, 166.44, 152.60, 150.67, 146.89, 132.61, 131.30, 130.90, 129.58, 128.50, 127.00, 125.48, 114.03, 113.13, 111.18, 97.81, 80.17, 70.19, 33.41, 24.97, 23.55, 17.58. HRMS (ESI) exact mass calcd for $C_{31}H_{33}O_6$ requires m/z 501.2277, found 501.2267.

4.1.2.10. (*Z*)-2-(4-(((2-(4-cyanobenzylidene)-3-oxo-2,3-dihydrobenzofuran-6-yl)oxy)methyl)-2,6-dimethylphenoxy)-2-methylpropanoic acid (10). 35% Yield, white solid. 1H NMR (500 MHz, DMSO- d_6) δ 12.89 (br s, 1H), 8.11 (s, 2H), 7.96 (s, 2H), 7.71 (d, $J = 8.0$ Hz, 1H), 7.25 (d, $J = 5.4$ Hz, 1H), 7.14 (d, $J = 6.3$ Hz, 2H), 7.01–6.85 (m, 2H), 5.15 (s, 2H), 2.21 (s, 6H), 1.39 (s, 6H). ^{13}C NMR (126 MHz, DMSO- d_6) δ 181.54, 175.08, 168.16, 166.80, 152.61, 148.60, 136.71, 132.63, 131.35, 130.80, 128.50, 125.75, 118.61, 113.54, 113.45, 111.36, 108.55, 97.95, 80.16, 70.28, 24.96, 17.57. HRMS (ESI) exact mass calcd for $C_{29}H_{25}NO_6Na$ requires m/z 506.1580, found 506.1569.

4.1.2.11. (*Z*)-2-(4-(((2-([1,1'-biphenyl]-4-ylmethylene)-3-oxo-2,3-dihydrobenzofuran-6-yl)oxy)methyl)-2,6-dimethylphenoxy)-2-methylpropanoic acid (11). 31% Yield, white solid. 1H NMR (500 MHz, DMSO- d_6) δ 12.88 (br s, 1H), 8.04 (d, $J = 8.0$ Hz, 2H), 7.80 (d, $J = 8.0$ Hz, 2H), 7.74 (d, $J = 7.5$ Hz, 2H), 7.69 (d, $J = 8.5$ Hz, 1H), 7.49 (t, $J = 7.4$ Hz, 2H), 7.41 (d, $J = 7.2$ Hz, 1H), 7.23 (s, 1H), 7.13 (s, 2H), 6.98–6.83 (m, 2H), 5.13 (s, 2H), 2.20 (s, 6H), 1.38 (s, 6H). ^{13}C NMR (126 MHz, DMSO- d_6) δ 181.53, 175.10, 167.88, 166.47, 152.59, 147.32, 141.17, 139.12, 132.61, 131.73, 131.11, 130.90, 129.00, 128.50, 128.01, 127.08, 126.73, 125.49, 113.98, 113.17, 110.60, 97.81, 80.15, 70.21, 24.96, 17.58. HRMS (ESI) exact mass calcd for $C_{34}H_{31}O_6$ requires m/z 535.2121, found 535.2108.

4.1.2.12. (*Z*)-2-(2,6-dimethyl-4-(((3-oxo-2-(2-(trifluoromethyl)benzylidene)-2,3-dihydrobenzofuran-6-yl)oxy)methyl)phenoxy)-2-methylpropanoic acid (12). 35% Yield, yellow solid. 1H NMR (500 MHz, DMSO- d_6) δ 12.90 (br s, 1H), 8.10 (d, $J = 8.0$ Hz, 2H), 7.80 (d, $J = 8.2$ Hz, 2H), 7.68 (d, $J = 8.5$ Hz, 1H), 7.18 (s, 1H), 7.12 (s, 2H), 6.97–6.83 (m, 2H), 5.12 (s, 2H), 2.20 (s, 6H), 1.38 (s, 6H). ^{13}C NMR (126 MHz, DMSO- d_6) δ 181.54, 175.09, 168.13, 166.72, 152.61, 148.30, 136.04, 132.63, 131.38, 130.84, 129.10 (q, $J = 31.5$ Hz), 128.45, 125.67, 125.60 (q, $J = 2.5$ Hz), 123.0 (q, $J = 273.4$ Hz), 113.62, 113.35, 108.73, 97.82, 80.15, 70.24, 64.89, 24.94, 17.56. HRMS (ESI) exact mass calcd for $C_{29}H_{26}F_3O_6$ requires m/z 527.1681, found 527.1673.

4.1.2.13. (*Z*)-2-(2,6-dimethyl-4-(((3-oxo-2-(4-(trifluoromethyl)benzylidene)-2,3-dihydro benzofuran-6-yl)oxy)methyl)phenoxy)-2-methylpropanoic acid (13). 28% Yield, white solid. 1H NMR (500 MHz, DMSO- d_6) δ 12.92 (br s, 1H), 8.36 (d, $J = 7.8$ Hz, 1H), 7.94–7.74 (m, 2H), 7.73 (d, $J = 8.5$ Hz, 1H), 7.65 (t, $J = 7.5$ Hz, 1H), 7.22 (s, 1H), 7.13 (s, 2H), 6.94 (d, $J = 8.2$ Hz, 1H), 6.85 (s, 1H), 5.13 (s, 2H), 2.20 (s, 6H), 1.38 (s, 6H). ^{13}C NMR (126 MHz, DMSO- d_6) δ 181.42, 175.09, 168.39, 166.90, 152.63, 148.50, 132.88, 132.63, 132.03, 130.78, 129.64, 129.48, 128.49, 127.70 (q, $J = 28.8$ Hz), 126.42 (q,

$J = 7.5$ Hz), 123.10 (q, $J = 274.6$ Hz), 113.48, 113.46, 103.84, 98.00, 80.17, 70.30, 24.96, 17.56. HRMS (ESI) exact mass calcd for $C_{29}H_{26}F_3O_6$ requires m/z 527.1681, found 527.1677.

4.1.2.14. (*Z*)-2-(2,6-dimethyl-4-(((3-oxo-2-(4-(trifluoromethoxy)benzylidene)-2,3-dihydrobenzofuran-6-yl)oxy)methyl)phenoxy)-2-methylpropanoic acid (14). 38% Yield, yellow solid. 1H NMR (500 MHz, DMSO- d_6) δ 12.90 (br s, 1H), 8.08 (d, $J = 8.0$ Hz, 2H), 7.71 (d, $J = 8.2$ Hz, 1H), 7.50 (d, $J = 7.6$ Hz, 2H), 7.21 (s, 1H), 7.13 (s, 2H), 7.02–6.82 (m, 3H), 5.14 (s, 2H), 2.21 (s, 6H), 1.38 (s, 6H). ^{13}C NMR (126 MHz, DMSO- d_6) δ 181.58, 175.10, 168.04, 166.62, 152.61, 148.75, 147.54, 132.94, 132.63, 131.32, 130.85, 128.49, 125.63, 121.31, 120.00 (q, $J = 257.0$ Hz), 113.80, 113.28, 109.19, 97.83, 80.17, 70.23, 24.96, 17.57. HRMS (ESI) exact mass calcd for $C_{29}H_{26}F_3O_7$ requires m/z 543.1631, found 543.1626.

4.1.2.15. (*Z*)-2-(2,6-dimethyl-4-(((3-oxo-2-(4-((trifluoromethyl)thio)benzylidene)-2,3-dihydrobenzofuran-6-yl)oxy)methyl)phenoxy)-2-methylpropanoic acid (15). 28% Yield, white solid. 1H NMR (500 MHz, DMSO- d_6) δ 12.88 (br s, 1H), 8.09 (d, $J = 7.4$ Hz, 2H), 7.84 (d, $J = 7.4$ Hz, 2H), 7.73 (d, $J = 8.2$ Hz, 1H), 7.24 (s, 1H), 7.14 (s, 2H), 7.00–6.79 (m, 2H), 5.15 (s, 2H), 2.21 (s, 6H), 1.39 (s, 6H). ^{13}C NMR (126 MHz, DMSO- d_6) δ 181.57, 175.07, 168.12, 166.74, 152.60, 148.29, 136.31, 134.98, 132.63, 132.01, 130.84, 129.40 (q, $J = 308.7$ Hz), 128.49, 125.72, 124.02, 113.68, 113.38, 108.95, 97.91, 80.16, 70.25, 24.95, 17.57. HRMS (ESI) exact mass calcd for $C_{29}H_{26}F_3SO_6$ requires m/z 559.1402, found 559.1392.

4.1.2.16. (*Z*)-2-(2,6-dimethyl-4-(((2-(naphthalen-2-ylmethylene)-3-oxo-2,3-dihydrobenzofuran-6-yl)oxy)methyl)phenoxy)-2-methylpropanoic acid (16). 37% Yield, white solid. 1H NMR (500 MHz, DMSO- d_6) δ 12.95 (br s, 1H), 8.52 (s, 1H), 8.19 (d, $J = 9.1$ Hz, 1H), 8.11–7.92 (m, 3H), 7.77 (d, $J = 8.4$ Hz, 1H), 7.65–7.55 (m, 2H), 7.35 (s, 1H), 7.17 (s, 2H), 7.05 (s, 1H), 6.98 (d, $J = 7.8$ Hz, 1H), 5.19 (s, 2H), 2.24 (s, 6H), 1.40 (s, 6H). ^{13}C NMR (126 MHz, DMSO- d_6) δ 181.60, 175.12, 168.00, 166.54, 152.64, 147.49, 133.11, 132.88, 132.63, 131.81, 130.87, 129.68, 128.49, 127.67, 127.58, 127.28, 126.84, 125.57, 113.97, 113.27, 111.07, 97.93, 80.22, 70.24, 25.01, 17.59. HRMS (ESI) exact mass calcd for $C_{32}H_{29}O_6$ requires m/z 509.1964, found 509.1952.

4.2. Molecular docking

All molecular docking procedures were completed in Schrödinger 2009. The crystal structures of PPAR- α (PDB ID: 4CI4) and PPAR- δ (PDB ID: 3SP9) obtained from RCSB (<http://www.rcsb.org>) were applied for molecular docking. The proteins in the crystal structures were prepared using the Protein Preparation Wizard workflow. The binding sites were defined with the crystal ligands in each crystal structure. Small molecules were prepared with LigPrep and then docked into the binding sites using the Glide module with extra precision (XP) mode.

4.3. In vivo evaluation

4.3.1. Materials and instruments

STZ was obtained from Sigma (USA). Ramipril was obtained from aladdin (Shanghai, China). Accu-Chek Active System was obtained from Roche (Germany). Rat metabolic cage was obtained from Zhenghua biologic apparatus facility (Huaibei, China). Test kits of albuminuria, urea nitrogen, creatinine, ALT, AST, MDA and SOD were obtained from Jiancheng Bioengineering Institute (Nanjing China). Test kits of cystatin C, TC, TG were obtained from Elabscience (Wuhan, China). Ts2R inverted fluorescence microscope was obtained from Nikon (Japan). Multimode plate reader was obtained

from PerkinElmer (USA). Trizol, PimeScript™ RT Master Mix (Perfect Real Time) and SYBR® Premix Ex Taq were obtained from Vazyme (Nanjing, China). BCA protein quantitative kit was obtained from Beyotime (Shanghai, China). Rat β -actin gene primer pair was obtained from Sangon (Shanghai, China). 4% paraformaldehyde, Anti-TGF- β 1 were obtained from Servicebio (Wuhan, China). Anti-collagen4 and anti-PPAR- δ were obtained from Proteintech (Wuhan, China). Anti-Phospho-JNK1/2/3, anti-JNK1/2/3, anti-Phospho-NF- κ B p65, anti-NF- κ B p65 were obtained from ABclonal (Wuhan, China). Anti- β -actin was obtained from arigo (Shanghai, China). HRP-labeled goat anti-mouse IgG secondary antibody was obtained from Fcmacs (Nanjing, China). HRP-labeled goat anti-rabbit IgG secondary antibody was obtained from CoWin (Beijing, China). Western blot detected kit (Tanon™ High-sig ECL Western Blotting Luminol/Enhancer Solution and Tanon™ High-sig ECL Western Blotting Peroxide Buffer) was obtained from Tanon Science & Technology Co., Ltd (Shanghai, China).

4.3.2. Animals

8-week-old male Sprague-Dawley rats were supplied by the Charles River Laboratory Animal Technology Co., Ltd. (Pinghu, China) (Certificate No. SCXK (Zhe) 2019-001). Experimental procedures involving the use of animals complied with the Guidelines for Animal Experimentation of the China Pharmaceutical University (Nanjing, China). The protocol was approved by the Animal Ethics Committee of that institution. All animals were maintained under standard environmental conditions and provided with feed and water *ad libitum*.

4.3.3. Establishment of rat models of DKD

After one week of acclimatization, rats were randomly assigned into control (n = 8) and model (n = 40) group. After fasting for 12 h, the rats of diabetes were induced by injecting a single dose of STZ (55 mg/kg, intraperitoneally) dissolved in ice-cold sodium citrate buffer (0.01 M, pH 4.4). The rats of control were received only sodium citrate buffer. After 3 days of STZ injection, peripheral blood was harvested from vena caudalis and measured by an Accu-Chek Active System, the fasting blood glucose between 16.7 mM and 33 mM were considered diabetes. Sequentially, each rat fasting blood glucose were measured, 24 h urine were collected using metabolic cage and the 24 h albuminuria were detected every week. The signs of fasting blood glucose between 16.7 mM and 33 mM, 24 h urine volume >150% raw urine, and 24 h albuminuria >30 mg can be seen as the successful establishment of the DKD rat model [52].

4.3.4. Experimental protocol

To intuitively compare the therapeutic efficacy with currently clinical drug (ACEI) for DKD, based on the fasting blood glucose and 24 h albuminuria, DKD rats were divided into four groups: model group, ramipril group (2 mg/kg, positive control), low dose compound **12** group (25 mg/kg) and high dose compound **12** group (50 mg/kg), 10 rats in each group. The dosages of compound **12** were consulted and optimized as described previously [19,23]. Ramipril, an ACEI, which can inhibit aldosterone secretion to exert favorable protective effects on renal functions in clinical practice and often used as positive control in the therapeutic efficacy for DKD [53]. All agents were prepared with carboxymethyl cellulose sodium (CMC-Na) as suspension (0.5%) and orally given for 6 weeks, in which compound **12** groups (both low group and high group) were gavaged twice a day and another groups were gavaged once a day. During the experiments, body weight was measured every week, fasting blood glucose and 24 h albuminuria were measured every two weeks. At the end of experiments, all rats were sacrificed and blood was obtained *via* orbital cavity, kidneys were

separated, the left kidney was stored in liquid nitrogen immediately and then stored at -80°C , the right kidney was photographed and weighed to calculate the ratio of kidney/body weight, then fixed in 4% paraformaldehyde for subsequent examinations.

4.3.5. Estimation of urine and serum biochemical parameters

Urine was obtained from each rat and centrifuged under 3000 rpm for 10 min. Levels of 24 h albuminuria in the supernatant were determined according to the protocol of urinary protein test kit. The blood was centrifuged at 3000 g for 15 min after 3 h at room temperature, serum was prepared and stored at -80°C until use. Serum levels of urea nitrogen, creatinine, cystatin C, TC, TG, ALT, AST, levels of serum and kidney MDA and SOD were determined using corresponding assay kits according to their protocols.

4.3.6. Renal histology analysis

The right kidney tissue samples were fixed in 4% paraformaldehyde, subjected to standard histological processing and embedded in paraffin. The sample was cut to 5 μm thick, stained with HE, PAS and Masson's trichrome following standard protocols. Lipid content in kidney was determined by Oil Red O staining with kidney frozen sections as described [54]. Briefly, frozen sections of kidney were rinsed with Oil Red O solution for 10 min in the dark. And then sections rinsed with 60% isopropanol for differentiation. Subsequently, sections were stained with hematoxylin solution, and then were sealed to slices with glycerin gelatin. Photographs were taken in a blinded fashion at random fields. Representative views of kidney sections were shown. Quantification of staining was performed using software Image J and was expressed as a percentage of the positive region [55]. All images were analyzed by two investigators blinded to the identity of the samples.

4.3.7. Immunohistochemistry analysis

Sections were dewaxed and rehydrated, followed by antigen retrieval, blocking with 3% H_2O_2 and BSA. After that, sections were incubated overnight with anti-TGF- β 1 (1:200) or anti-collagen4 (1:500) in a humidified chamber at 4°C . The sections were washed with PBS and exposed to secondary antibody (HRP-labeled) from the corresponding species of primary antibody and incubated at room temperature for 50 min. Meanwhile, negative control was set up. Diaminobenzidine (DAB) was used as a chromogen. The positive (stained) area for each marker was calculated using colour thresholding and by measuring area fractions with software Image J [55]. All images were analyzed by two investigators blinded to the identity of the samples.

4.3.8. Reverse transcription-polymerase chain reaction (RT-PCR)

The RT-PCR analysis were performed as described previously [56]. Briefly, total RNA was extracted from 10 mg of the renal cortex using 500 μL Trizol according to the manufacturer's instructions. One microgram of total RNA was reverse transcribed into cDNA using HiScript II Q RT SuperMix kit according to the manufacturer's protocol. The Power SYBR Green Master Mix was used for real-time PCR analysis. Differences in gene expression between groups were calculated using cycle threshold (Ct) values. Relative expression of genes was calculated by the $2^{-\Delta\Delta\text{Ct}}$ method. The necessary primers were purchased from Sangon and all primer pairs could be seen in the supplementary data (Table S1). Gene expression values were normalized to the expression levels of β -actin.

4.3.9. Western blotting analysis

The Western blot analysis were performed as described previously [57]. Briefly, a piece of the renal cortex were lysed using a lysis buffer [120 mM NaCl, 1% NP-40, 0.5% sodium deoxycholate, 0.1% SDS, 50 mM Tris-HCl (pH 7.6)], and proteins were obtained after

centrifugation. The concentrations of proteins were determined using a BCA protein assay kit. The equal amounts of proteins were then electrophoresed on 10% SDS polyacrylamide gels. After transferring to PVDF membranes, the membranes were blocked with a 5% BSA solution for 1 h and incubated overnight with primary antibodies. Then membranes were incubated continually with secondary antibodies, and the bands were detected using a Western blot detection kit.

4.4. *In vitro* evaluation

4.4.1. Evaluation for PPARs agonist activities

4.4.1.1. Materials. COS7 cell was obtained from Cellcook (Guangzhou, China). Dulbecco's modified Eagle medium (DMEM), fetal bovine serum (FBS), and penicillin-streptomycin solution were obtained from Biological Industries (Israel). The pGL4.35 with $9 \times \text{Gal4}$ UAS Luc reporter plasmid was purchased from Promega (USA). Opti-MEM was obtained from Gibco (USA). Transfection reagent was obtained from ABclonal (Wuhan, China). Firefly luciferase reporter gene assay kit was obtained from Beyotime (Shanghai, China).

4.4.1.2. Plasmids. The cDNA sequences of human PPARs ligand-binding domain were subcloned to pBIND vector to construct chimeric human PPARs-Gal4 receptor expression plasmids. Site-specific mutants of PPARs-Gal4 were generated by PCR-based, site-directed mutagenesis kit according to the manufacturer's instructions [58].

4.4.1.3. Cell culture and transactivation assay. COS7 cells were cultured in DMEM supplemented with 10% FBS and 1% penicillin-streptomycin solution. The main function of PPARs relies on its transcriptional activity, which is regulated by the ligand binding to PPARs ligand-binding domain (LBD). Detailed descriptions on transfection and cell-based evaluation for PPAR- α , PPAR- δ and PPAR- γ were given in our previously reported literature [58]. Briefly, COS7 cells were transfected with expression plasmids encoding the fusion protein GAL4-PPAR- α -LBD, GAL4-PPAR- δ -LBD or GAL4-PPAR- γ -LBD, mixed with transfection reagent in Opti-MEM according to the manufacturer's instruction. 4 h after transfection, cells were distributed in 96-well plates to recover for 24 h. After an overnight incubation, the three luciferase activities were measured using firefly luciferase reporter gene assay kit on a multimode plate reader, respectively. Dose-response curves were constructed with GraphPad Prism version 8.0 to determine the EC₅₀ value.

4.4.2. Evaluation for pharmacological activity in HGMCs and THP-1-derived macrophages

4.4.2.1. Materials. HGMCs were obtained and maintained according to distributor guidelines from ScienCell Research Laboratories (USA). THP-1 cells were obtained from Stem Cell Bank, Chinese Academy of Sciences, Roswell Park Memorial Institute-1640 (RPMI-1640) medium was obtained from Biological Industries (Israel). Recombinant human TGF- β 1 was obtained from Peprtech (USA). Phorbol 12-myristate 13-acetate (PMA) was obtained from MedChemExpress (USA). Dimethyl sulfoxide (DMSO) and LPS were obtained from Sigma (USA). Cell Counting Kit-8 (CCK-8) was obtained from Beyotime (Shanghai, China). Human β -actin gene primer pair was obtained from Sangon (Shanghai, China).

4.4.2.2. Cell culture and intervention. HGMCs were cultured in DMEM (containing 5.5 mM of D-glucose) supplemented with 10% FBS and 1% penicillin-streptomycin solution and were used in passage of 6–10. THP-1 cells were cultured in RPMI-1640 medium

supplemented with 10% FBS and 1% penicillin-streptomycin solution. For the experiments, HGMCs were plated in 6-well dishes at a density of 2×10^5 cells/well overnight, and then were incubated with serum-free medium for 24 h to arrest and synchronize cell growth. THP-1 cells were plated in 12-well dishes at a density of 5×10^5 cells/well, and then were treated with 100 ng/mL PMA to differentiate. After 48 h, differentiated THP-1 cells were washed with PBS twice and rested for another 24 h in the culture medium to obtain the resting state of macrophage. For the RT-PCR analysis, HGMCs were exposed in 5.5 mM D-glucose (low glucose, as control), 30 mM D-glucose (high glucose, HG) or 5.5 mM D-glucose plus 24.5 mM mannitol (as an osmotic control for 30 mM D-glucose) with or without the additional 24 h application of the compound **12** at different concentrations (1, 3 or 10 μM). Meanwhile, HGMCs were exposed in 10 ng/mL TGF- β 1 with or without the additional 6 h application of the compound **12** at different concentrations (1, 3 or 10 μM). The differentiated THP-1 cells were treated with 100 ng/mL LPS or LPS plus the compound **12** at different concentrations (1, 3 or 10 μM) for 6 h. For the Western blot analysis, cells were pre-incubated with compound **12** at different concentrations (1, 3 or 10 μM) for 2 h followed by post incubation with HG or LPS for 0.5 h.

4.4.2.3. Cell viability test. Cell viability was determined using the CCK-8 assay. HGMCs (1×10^4 cells/well) were incubated in a 96-well plate in DMEM (containing 5.5 mM of D-glucose) supplemented with 10% FBS and 1% penicillin-streptomycin solution. After culturing overnight, HGMCs were starved in serum-free DMEM for 24 h. THP-1 cells (4×10^5 cells/well) were seeded in 96-well plate in RPMI-1640 containing 10% FBS and 100 ng/mL PMA to differentiate. After 48 h, differentiated THP-1 cells were washed with PBS twice and rested for another 24 h in the culture medium to obtain the resting state of macrophage. After that, two types of cells were exposed to compound **12** at different concentrations (0, 1, 3, 10, 30 μM) for 48 h, CCK-8 solution (10 μL) was then added to each well, followed by incubation for 1 h. Absorbance at 450 nm was measured.

4.5. Statistical analysis

All data are presented as the means \pm SEM, and analyses were performed with Graphpad Prism 8 software. Comparisons between experimental groups were conducted using One-way ANOVA. Values of $p < 0.05$ were considered significant.

Declaration of competing interest

The authors declare that they have no known competing financial interests or personal relationships that could have appeared to influence the work reported in this paper.

Acknowledgements

Financial support from National Natural Science Foundation of China (grants 21971256, 21977118 and 81773584) is gratefully acknowledged. This project was also supported by the Jiangsu Provincial Key Research and Development Project (BE2018710), the "Double First-Class" University project (CPU2018GY01, CPU2018GY35, CPU2018GY45) and the Program for Jiangsu Province Innovative Research Team. The authors appreciated Jie Zhao, who works in the pharmaceutical animal experimental center of China Pharmaceutical University, for her kind help in the animal feeding.

Appendix A. Supplementary data

Supplementary data to this article can be found online at <https://doi.org/10.1016/j.ejmech.2021.113388>.

References

- [1] K. Tuttle, The landscape of diabetic kidney disease transformed, *Nat. Rev. Nephrol.* 16 (2020) 67–68, <https://doi.org/10.1038/s41581-019-0240-6>.
- [2] S. Jiang, J. Fang, T. Yu, W. Li, Angiotensin-converting enzyme inhibitors versus angiotensin II receptor blockers for renal outcomes and mortality in diabetic kidney disease, *Eur. J. Intern. Med.* 85 (2021) 127–129, <https://doi.org/10.1016/j.ejim.2020.11.017>.
- [3] P. Rossing, J. Strand, A. Avogaro, M. Becka, F. Kanefendt, C. Otto, Effects of the chymase inhibitor fulacimstat in diabetic kidney disease—results from the CADA DIA trial, *Nephrol. Dial. Transplant.* (2020) gfaa299, <https://doi.org/10.1093/ndt/gfaa299>.
- [4] R. Alicic, E. Cox, J. Neumiller, K. Tuttle, Incretin drugs in diabetic kidney disease: biological mechanisms and clinical evidence, *Nat. Rev. Nephrol.* (2020), <https://doi.org/10.1038/s41581-020-00367-2>. Online ahead of print.
- [5] R. Nakamichi, K. Hayashi, H. Itoh, Effects of high glucose and lipotoxicity on diabetic podocytes, *Nutrients* 13 (2021) 241, <https://doi.org/10.3390/nu13010241>.
- [6] E. Dozio, S. Vettoretti, L. Caldiroli, S. Nerini-Molteni, L. Tacchini, F. Ambrogi, P. Messa, M. Corsi Romanelli, Advanced glycation end products (AGE) and soluble forms of AGE receptor: emerging role as mortality risk factors in CKD, *Biomedicines* 8 (2020) 638, <https://doi.org/10.3390/biomedicines8120638>.
- [7] D. Cherney, A. Konvalinka, B. Zinman, E. Diamandis, A. Soosaipillai, H. Reich, J. Lorraine, V. Lai, J. Scholey, J. Miller, Effect of protein kinase Cbeta inhibition on renal hemodynamic function and urinary biomarkers in humans with type 1 diabetes: a pilot study, *Diabetes Care* 32 (2009) 91–93, <https://doi.org/10.2337/dc08-1609>.
- [8] A. Beyer-Mears, The polyol pathway, sorbinil, and renal dysfunction, *Metabolism* 35 (1986) 46–54, [https://doi.org/10.1016/0026-0495\(86\)90187-3](https://doi.org/10.1016/0026-0495(86)90187-3).
- [9] J. Lovshin, G. Boulet, Y. Lytvyn, L. Lovblom, P. Bjornstad, M. Farooqi, V. Lai, L. Cham, J. Tse, A. Orszag, D. Scarr, A. Weisman, H. Keenan, M. Brent, N. Paul, V. Bril, B. Perkins, D. Cherney, Renin-angiotensin-aldosterone system activation in long-standing type 1 diabetes, *JCI insight* 3 (2018), e96968, <https://doi.org/10.1172/jci.insight.96968>.
- [10] J. Lin, R. Glynn, N. Rifai, J. Manson, P. Ridker, D. Nathan, D. Schaumberg, Inflammation and progressive nephropathy in type 1 diabetes in the diabetes control and complications trial, *Diabetes Care* 31 (2008) 2338–2343, <https://doi.org/10.2337/dc08-0277>.
- [11] K. Sharma, Obesity, oxidative stress, and fibrosis in chronic kidney disease, *Kidney Int. Suppl.* 4 (2014) 113–117, <https://doi.org/10.1038/kisup.2014.21>.
- [12] P. Brown, T. Smith-Oliver, P. Charifson, N. Tomkinson, A. Fivush, D. Sternbach, L. Wade, L. Orband-Miller, D. Parks, S. Blanchard, S. Kliever, J. Lehmann, T. Willson, Identification of peroxisome proliferator-activated receptor ligands from a biased chemical library, *Chem. Biol.* 4 (1997) 909–918, [https://doi.org/10.1016/s1074-5521\(97\)90299-4](https://doi.org/10.1016/s1074-5521(97)90299-4).
- [13] N. Broeders, D. Abramowicz, Peroxisome proliferator-activated receptors (PPARs): novel therapeutic targets in renal disease, *Kidney Int.* 61 (2002) 354–355, <https://doi.org/10.1046/j.1523-1755.2002.00129.x>.
- [14] J. Wilding, PPAR agonists for the treatment of cardiovascular disease in patients with diabetes, *Diabetes Obes. Metabol.* 14 (2012) 973–982, <https://doi.org/10.1111/j.1463-1326.2012.01601.x>.
- [15] Y. Matsushita, D. Ogawa, J. Wada, N. Yamamoto, K. Shikata, C. Sato, H. Tachibana, N. Toyota, H. Makino, Activation of peroxisome proliferator-activated receptor delta inhibits streptozotocin-induced diabetic nephropathy through anti-inflammatory mechanisms in mice, *Diabetes* 60 (2011) 960–968, <https://doi.org/10.2337/db10-1361>.
- [16] P. Sarafidis, P. Stafylas, P. Georgianos, A. Saratzis, A. Lasaridis, Effect of thiazolidinediones on albuminuria and proteinuria in diabetes: a meta-analysis, *Am. J. Kidney Dis.* 55 (2010) 835–847, <https://doi.org/10.1053/j.ajkd.2009.11.013>.
- [17] A. Lincoff, J. Tardif, G. Schwartz, S. Nicholls, L. Rydén, B. Neal, K. Malmberg, H. Wedel, J. Buse, R. Henry, A. Weichert, R. Cannata, A. Svensson, D. Volz, D. Grobbee, Effect of alogliptin on cardiovascular outcomes after acute coronary syndrome in patients with type 2 diabetes mellitus: the AlCardio randomized clinical trial, *J. Am. Med. Assoc.* 311 (2014) 1515–1525, <https://doi.org/10.1001/jama.2014.3321>.
- [18] L. Liu, C. Liu, M. Zhao, Q. Zhang, Y. Lu, P. Liu, H. Yang, J. Yang, X. Chen, Y. Yao, The pharmacodynamic and differential gene expression analysis of PPAR α / δ agonist GFT505 in CDAHFD-induced NASH model, *PLoS One* 15 (2020), e0243911, <https://doi.org/10.1371/journal.pone.0243911>.
- [19] R. Hanf, L. Millatt, B. Cariou, B. Noel, G. Rigou, P. Delaitaille, V. Daix, D. Hum, B. Staels, The dual peroxisome proliferator-activated receptor alpha/delta agonist GFT505 exerts anti-diabetic effects in db/db mice without peroxisome proliferator-activated receptor gamma-associated adverse cardiac effects, *Diabetes Vasc. Dis. Res.* 11 (2014) 440–447, <https://doi.org/10.1177/1479164114548027>.
- [20] M. Song, G. Jeong, K. Kwon, S. Ka, H. Jang, J. Park, Y. Kim, B. Park, Sulfuretin protects against cytokine-induced beta-cell damage and prevents streptozotocin-induced diabetes, *Exp. Mol. Med.* 42 (2010) 628–638, <https://doi.org/10.3858/emm.2010.42.9.062>.
- [21] S. Kim, N. Song, S. Chang, G. Bahn, Y. Choi, D. Rhee, U. Yun, J. Choi, J. Lee, J. Yoo, D. Shin, K. Park, H. Kang, S. Lee, J. Ku, Y. Cho, K. Park, Sulfuretin prevents obesity and metabolic diseases in diet induced obese mice, *Biomol. Ther. (Seoul)* 27 (2019) 107–116, <https://doi.org/10.4062/biomolther.2018.090>.
- [22] Y. Lu, Y. Xiao, Y. Li, J. Li, F. Nan, J. Li, Sulfuretin protects hepatic cells through regulation of ROS levels and autophagic flux, *Acta Pharmacol. Sin.* 40 (2019) 908–918, <https://doi.org/10.1038/s41401-018-0193-5>.
- [23] K. Roh, S. Kim, H. Kang, J. Ku, K. Park, S. Lee, Sulfuretin has therapeutic activity against acquired lymphedema by reducing adipogenesis, *Pharmacol. Res.* 121 (2017) 230–239, <https://doi.org/10.1016/j.phrs.2017.05.003>.
- [24] R. Lamichhane, S. Kim, S. Kang, K. Lee, P. Pandeya, H. Jung, Exploration of underlying mechanism of anti-adipogenic activity of sulfuretin, *Biol. Pharm. Bull.* 40 (2017) 1366–1373, <https://doi.org/10.1248/bpb.b17-00049>.
- [25] L. Opazo-Rios, S. Mas, G. Marín-Royo, S. Mezzano, C. Gómez-Guerrero, J. Moreno, J. Egido, Lipotoxicity and diabetic nephropathy: novel mechanistic insights and therapeutic opportunities, *Int. J. Mol. Sci.* 21 (2020) 2632, <https://doi.org/10.3390/ijms21072632>.
- [26] P. Karabowicz, A. Wroński, H. Ostrowska, G. Waeg, N. Zarkovic, E. Skrzydlewska, Reduced proteasome activity and enhanced autophagy in blood cells of psoriatic patients, *Int. J. Mol. Sci.* 21 (2020) 7608, <https://doi.org/10.3390/ijms21207608>.
- [27] J. Forbes, M. Coughlan, M. Cooper, Oxidative stress as a major culprit in kidney disease in diabetes, *Diabetes* 57 (2008) 1446–1454, <https://doi.org/10.2337/db08-0057>.
- [28] Y. Liang, S. Chen, J. Jian, Peroxisome proliferator-activated receptor δ down-regulates the expression of the receptor for advanced glycation end products and pro-inflammatory cytokines in the kidney of streptozotocin-induced diabetic mice, *Eur. J. Pharmacol.* 43 (2011) 65–70, <https://doi.org/10.1016/j.ejps.2011.03.011>.
- [29] M. Murakami, J. Suzuki, S. Yamazaki, M. Ikezoe, R. Matsushima, N. Ashigaki, N. Aoyama, N. Kobayashi, K. Wakayama, H. Akazawa, I. Komuro, Y. Izumi, M. Isohe, High incidence of Aggregatibacter actinomycetemcomitans infection in patients with cerebral infarction and diabetic renal failure: a cross-sectional study, *BMC Infect. Dis.* 13 (2013) 557, <https://doi.org/10.1186/1471-2334-13-557>.
- [30] V. D'Agati, S. Yan, R. Ramasamy, A. Schmidt, RAGE, glomerulosclerosis and proteinuria: roles in podocytes and endothelial cells, *Trends. Endocrinol. Metab.* 21 (2010) 50–56, <https://doi.org/10.1016/j.tem.2009.07.003>.
- [31] E. Lee, G. Kim, M. Hyun, S. Kim, S. Seok, R. Choi, M. Lee, C. Chung, Peroxisome proliferator-activated receptor- δ activation ameliorates albuminuria by preventing nephrin loss and restoring podocyte integrity in type 2 diabetes, *Nephrol. Dial. Transplant.* 27 (2012) 4069–4079, <https://doi.org/10.1093/ndt/gfs358>.
- [32] D. Wang, J. Mann, R. DuBois, WNT and cyclooxygenase-2 cross-talk accelerates adenoma growth, *Cell Cycle* 3 (2004) 1512–1515, <https://doi.org/10.4161/cc.3.12.1288>.
- [33] Z. Kunicka, A. Kurzyńska, A. Szydłowska, B. Kaczyńska, I. Bogacka, PPAR β / δ ligands regulate the expression of immune response mediators in the porcine endometrium - an in vitro study, *Theriogenology* 134 (2019) 112–120, <https://doi.org/10.1016/j.theriogenology.2019.05.022>.
- [34] S. Sinha, M. Shaheen, T. Rajavashisth, D. Pan, K. Norris, S. Nicholas, Association of race/ethnicity, inflammation, and albuminuria in patients with diabetes and early chronic kidney disease, *Diabetes Care* 37 (2014) 1060–1068, <https://doi.org/10.2337/dc13-0013>.
- [35] E. Xiang, B. Han, Q. Zhang, W. Rao, Z. Wang, C. Chang, Y. Zhang, C. Tu, C. Li, D. Wu, Human umbilical cord-derived mesenchymal stem cells prevent the progression of early diabetic nephropathy through inhibiting inflammation and fibrosis, *Stem Cell Res. Ther.* 11 (2020) 336, <https://doi.org/10.1186/s13287-020-01852-y>.
- [36] I. Tuleta, N. Frangogiannis, Diabetic fibrosis, *Biochim. Biophys. Acta (BBA) - Mol. Basis Dis.* 1867 (2020) 166044, <https://doi.org/10.1016/j.jbbadis.2020.166044>.
- [37] P. Boor, T. Ostendorf, J. Floege, Renal fibrosis: novel insights into mechanisms and therapeutic targets, *Nat. Rev. Nephrol.* 6 (2010) 643–656, <https://doi.org/10.1038/nrneph.2010.120>.
- [38] Y. Ito, J. Aten, R. Bende, B. Oemar, T. Rabelink, J. Weening, R. Goldschmeding, Expression of connective tissue growth factor in human renal fibrosis, *Kidney Int.* 53 (1998) 853–861, <https://doi.org/10.1111/j.1523-1755.1998.00820.x>.
- [39] X. Meng, D. Nikolic-Paterson, H. Lan, TGF- β : the master regulator of fibrosis, *Nat. Rev. Nephrol.* 12 (2016) 325–338, <https://doi.org/10.1038/nrneph.2016.48>.
- [40] Y. Jiang, F. Xie, X. Lv, S. Wang, X. Liao, Y. Yu, Q. Dai, Y. Zhang, J. Meng, G. Hu, Z. Peng, L. Tao, Mefenidone ameliorates diabetic kidney disease in STZ and db/db mice, *Faseb. J.* 35 (2021), e21198, <https://doi.org/10.1096/fj.202001138RR>.
- [41] Y. Kanwar, J. Wada, L. Sun, P. Xie, E. Wallner, S. Chen, S. Chugh, F. Danesh, Diabetic nephropathy: mechanisms of renal disease progression, *Exp. Biol. Med.* 233 (2008) 4–11, <https://doi.org/10.3181/0705-mr-134>.
- [42] X. Ruan, F. Zheng, Y. Guan, PPARs and the kidney in metabolic syndrome, *Am. J. Physiol. Ren. Physiol.* 294 (2008) F1032–F1047, <https://doi.org/10.1152/ajprenal.00152.2007>.
- [43] H. Yari Beygi, M. Mohammadi, R. Rezaee, A. Sahebkar, Fenofibrate improves renal function by amelioration of NOX-4, IL-18, and p53 expression in an experimental model of diabetic nephropathy, *J. Cell. Biochem.* 119 (2018)

- 7458–7469, <https://doi.org/10.1002/jcb.27055>.
- [44] N. Al-Rasheed, N. Al-Rasheed, M. Al-Amin, I. Hasan, H. Al-Ajmi, R. Mohammad, H. Attia, Fenofibrate attenuates diabetic nephropathy in experimental diabetic rat's model via suppression of augmented TGF- β 1/Smad 3 signaling pathway, *Arch. Physiol. Biochem.* 122 (2016) 186–194, <https://doi.org/10.3109/13813455.2016.1164186>.
- [45] L. Czupryniak, S. Joshi, J. Gogtay, M. Lopez, Effect of micronized fenofibrate on microvascular complications of type 2 diabetes: a systematic review, *Expet Opin. Pharmacother.* 17 (2016) 1463–1473, <https://doi.org/10.1080/14656566.2016.1195811>.
- [46] F. Emami, A. Hariiri, M. Matinfar, M. Nematbakhsh, Fenofibrate-induced renal dysfunction, yes or no? *J. Res. Med. Sci.* 25 (2020) 39, https://doi.org/10.4103/jrms.JRMS_772_19.
- [47] W. Hu, Q. Yu, J. Zhang, D. Liu, Rosiglitazone ameliorates diabetic nephropathy by reducing the expression of Chemerin and ChemR23 in the kidney of streptozotocin-induced diabetic rats, *Inflammation* 35 (2012) 1287–1293, <https://doi.org/10.1007/s10753-012-9440-y>.
- [48] A. Bézardeau, P. Verry, E. Atzpodien, J. Funk, M. Meyer, J. Mizrahi, M. Winter, M. Wright, S. Uhles, E. Sebkova, Effects of the dual PPAR- α/γ agonist aleglitazar on glycaemic control and organ protection in the Zucker diabetic fatty rat, *Diabetes Obes. Metabol.* 15 (2013) 164–174, <https://doi.org/10.1111/dom.12006>.
- [49] M. Soltsova Prnova, M. Majekova, I. Milackova, B. Díez-Dacal, D. Pérez-Sala, M. Ceyhan, S. Banerjee, M. Stefek, [5-(Benzyloxy)-1H-indol-1-yl]acetic acid, an aldose reductase inhibitor and PPAR γ ligand, *Acta Biochim. Pol.* 62 (2015) 523–528, https://doi.org/10.18388/abp.2014_953.
- [50] H. Sullivan, X. Wang, S. Nogle, S. Liao, C. Wu, To probe full and partial activation of human peroxisome proliferator-activated receptors by pan-agonist chiglitazar using molecular dynamics simulations, *PPAR Res.* 2020 (2020) 5314187, <https://doi.org/10.1155/2020/5314187>.
- [51] B. Cariou, B. Charbonnel, B. Staels, Thiazolidinediones and PPAR γ agonists: time for a reassessment, *Trends Endocrinol. Metabol.* 23 (2012) 205–215, <https://doi.org/10.1016/j.tem.2012.03.001>.
- [52] C. Chen, J. Lin, L. Li, T. Zhu, L. Gao, W. Wu, Q. Liu, S. Ou, The role of the BMP4/Smad 1 signaling pathway in mesangial cell proliferation: a possible mechanism of diabetic nephropathy, *Life Sci.* 220 (2019) 106–116, <https://doi.org/10.1016/j.lfs.2019.01.049>.
- [53] S. Malik, K. Suchal, S. Khan, J. Bhatia, K. Kishore, A. Dinda, D. Arya, Apigenin ameliorates streptozotocin-induced diabetic nephropathy in rats via MAPK-NF- κ B-TNF- α and TGF- β 1-MAPK-fibronectin pathways, *Am. J. Physiol. Ren. Physiol.* 313 (2017) F414–F422, <https://doi.org/10.1152/ajprenal.00393.2016>.
- [54] S. Yang, C. Ma, H. Wu, H. Zhang, F. Yuan, G. Yang, Q. Yang, L. Jia, Z. Liang, L. Kang, Tectorigenin attenuates diabetic nephropathy by improving vascular endothelium dysfunction through activating AdipoR1/2 pathway, *Pharmacol. Res.* 153 (2020) 104678, <https://doi.org/10.1016/j.phrs.2020.104678>.
- [55] S. Udi, L. Hinden, M. Ahmad, A. Drori, M. Iyer, R. Cinar, M. Herman-Edelstein, J. Tam, Dual inhibition of cannabinoid CB receptor and inducible NOS attenuates obesity-induced chronic kidney disease, *Br. J. Pharmacol.* 177 (2020) 110–127, <https://doi.org/10.1111/bph.14849>.
- [56] L. Liu, H. Li, K. Hu, Q. Xu, X. Wen, K. Cheng, C. Chen, H. Yuan, L. Dai, H. Sun, Synthesis and anti-inflammatory activity of saponin derivatives of δ -oleanolic acid, *Eur. J. Med. Chem.* 209 (2021) 112932, <https://doi.org/10.1016/j.ejmech.2020.112932>.
- [57] K. Liu, H. Xu, G. Lv, B. Liu, M. Lee, C. Lu, X. Lv, Y. Wu, Loganin attenuates diabetic nephropathy in C57BL/6J mice with diabetes induced by streptozotocin and fed with diets containing high level of advanced glycation end products, *Life Sci.* 123 (2015) 78–85, <https://doi.org/10.1016/j.lfs.2014.12.028>.
- [58] L. Dai, Z. Feng, R. Zha, K. Cheng, X. Wen, H. Sun, H. Yuan, Discovery of novel peroxisome proliferator-activated receptor α (PPAR α) agonists by virtual screening and biological evaluation, *J. Chem. Inf. Model.* 60 (2020) 1717–1727, <https://doi.org/10.1021/acs.jcim.9b00838>.